DOI: 10.1002/ ((please add manuscript number))

Article type: Review

Recent advances in graphene homogeneous p-n junction for optoelectronics

Pin Tian[1], Libin Tang[1], Kar Seng Teng[2],* Jinzhong Xiang[3], and Shu Ping Lau[4]**

[1] Kunming Institute of Physics, 650223, Kunming, Yunnan, China.

[2] College of Engineering, Swansea University, Bay Campus, Fabian Way, Swansea SA1 8EN, United Kingdom.

[3] Yunnan University, School of Physics and Astronomy, 650091, Kunming, Yunnan, China.

[4] The Hong Kong Polytechnic University, Department of Applied Physics, Hung Hom, Kowloon, Hong Kong, China.

E-mail: scitang@163.com (L.B. Tang), k.s.teng@swansea.ac.uk(K.S. Teng) and apsplau@polyu.edu.hk (S.P. Lau)

Keywords: Graphene, homogeneous p-n junction, p- and n-type graphene, optoelectronics.

Graphene has been widely used as electrodes and active layers in optoelectronics due to its diverse excellent performances, such as high mobility, large thermal conductivity and high specific surface area etc. Methodology for constructing p-n junction has becoming an important consideration in improving the performance of optoelectronic devices and broadening of its application in related fields. Currently, graphene based p-n junction has been explored and different structures have also been investigated. This review paper summaries the recent progress on graphene homogeneous p-n junction, ranging from preparation of front-end materials (e.g. p- and n-type graphene) to building of planar and vertical p-n junctions. Furthermore, p-n junction via electrical modulation is described. The requirements for building the graphene homogeneous p-n junction, and the advantages and drawbacks of the different structures of the p-n junction are also discussed. Finally, a preferential technique to fabricate high performance p- and n-type graphene and building of the p-n junction is evaluated. This paper therefore provides an important indication on the future direction on the application of graphene in optoelectronics.

1. Introduction

Traditional silicon-based semiconductor is facing enormous technological challenges due to the continuous demands on the enhancement of device performances. Thus, it is necessary for the exploration of novel semiconductor materials and study of its exotic properties.[1] These materials will potentially transform the performances of current electronic devices or lead to the development of novel devices, such as graphene[2-5], TMDs[6,7] and black phosphorus[8,9] and so on. One of the most basic semiconductor devices is the p-n junction, which has crucial role in wide ranging applications, such as logical rectifier circuit[10,11], field-effect optoelectronic transistor[12-14], multimode non-volatile memory[15], rectifier memory[16,17], optoelectronic storage[18,19], photovoltaic device[20], photodetector[21,22] and gas sensor[23,24] etc. Consequently, it becomes important to study new material system for the p-n junction that will enhance the performance of those devices and also lead to the development of new devices. In general, p-n junction can be categorized into heterojunction and homojunction. If same materials are used, the p-n junction is known as homogeneous junction or homojunction. There are many advantages of homogeneous p-n junction, for example, there is no issue on lattice mismatch, which will result in surface defects, since p and n layers are of the same materials. Moreover, the use of the same materials in homogeneous p-n junction leads to uniform energy band gap across the device structure, as shown in Figure 1a. Depletion region is formed at the junction between p and n regions, and the unification of Fermi level (E_f) promotes band bending at the depletion region when the same semiconducting materials are used to construct the p-n junction, as represented in Figure 1b. Such homogeneous p-n junction is of great significance in the field of optoelectronics. Figure 1c illustrates the charge transport mechanism under illumination. Upon radiation of light with certain wavelength ($h\upsilon \geqq Eg$), electrons jump to conduction band in p, n and depletion regions. These electrons and holes arriving at the depletion region are subsequently swept into n-type and p-type regions respectively via the built-in field. As a result, current is generated and a certain voltage is produced due to the accumulation of charges under open circuit conditions. Furthermore, this leads to narrowing of the depletion width and modification of the

Fermi level because of charge variation during the process of current generation for traditional semiconductors. The p-n junction, and its materials and structures are therefore critical to the performance of photovoltaic devices. As graphene is one of the important discoveries in the beginning of the 21st century, it is of scientific interest to develop p-n junction based on this exciting material.

Graphene is an atomically thin single layer of carbon atoms covalently bond in a honeycomb lattice,[25] as depicted in the bottom left image of Figure 1d. However, the properties of graphene are reflected by its structure. The p_z orbital on each carbon atoms overlaps with nearby carbon atoms to generate a filled band of π orbitals which is known as the valence band. An unoccupied band of π^* orbitals, which is known as the conduction band, is due to the *s*, p_x and p_y atomic orbitals on each carbon atom in graphene forming three strong σ bonds with three other neighbouring atoms.[26] When the valence and conduction bands touch at 6 points in K-space which can be grouped in two inequivalent sets, in undoped graphene the Fermi energy sits at the neutrality point which corresponds to the touching point between the two bands, the Fermi level of graphene is located near the Dirac point and hence resulting in gapless energy band.[27] Those structural characteristics indicate that graphene could exhibit some exotic physical characteristics, such as good flexibility, high mechanical strength (tensile strength and modulus of elasticity are 125 GPa and 1.1 TPa,[28] respectively), high carriers mobility (2×10^5 $cm^2V^{-1}s^{-1}$),[29] high optical transmission (transmissivity is up to 97.7%)[30] and excellent thermal conductivity (up to 5×10^3 $Wm^{-1}K^{-1}$)[31] etc. However, these properties have ill-effect on the application of graphene in optoelectronics due to its zero band gap, lower optical absorbance and poor carrier separation efficiency etc. Hence, there is a need to tailor the properties of graphene for its novel application in optoelectronics. To date, numerous studies have been performed to address these challenges and have gained fruitful achievements on energy band engineering via doping or tailored methods (see in Figure 1d)[32-48] or conductive type modulation[49-53] of graphene. Doping can shift the Fermi energy in the conduction or valence band (by selecting appropriate dopants) and the band gap of graphene, while the tailored approach can control the size of gap by controlling the size and shape of graphene-derivatives, such as

graphene quantum dots[39,54,55] and graphene nanoribbons[56-58] etc. It has been suggested that the internal quantum efficiency of graphene can be enhanced through the use of graphene homogeneous p-n junction [59,60]. Besides, many exotic physical phenomenon can be observed in the graphene homogenous p-n junction due to graphene's unique properties, such as important Klein tunneling effect, which was predicted by Oskar Klein[61] in 1929 and realized in recent experiment[62] of graphene homogenous p-n junction. The research interest of graphene p-n junction has experienced an exponential growth due to its technological importance

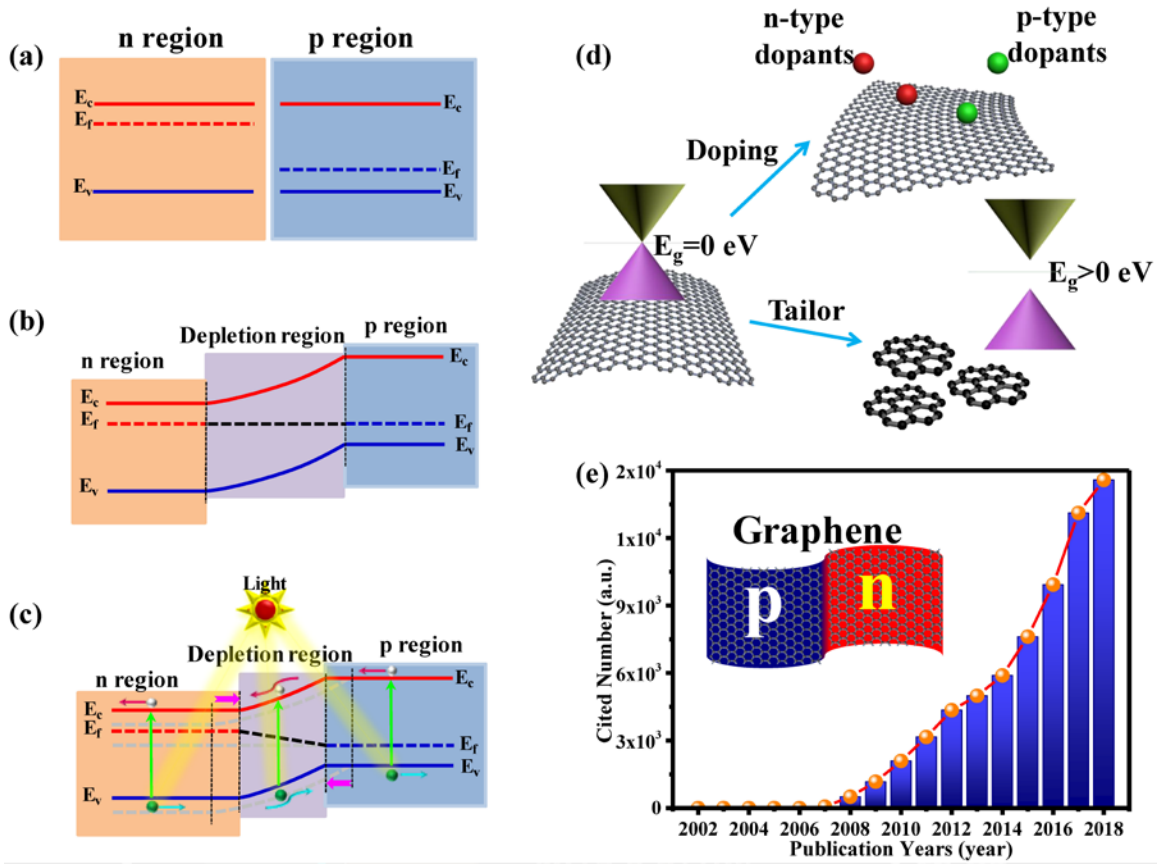

Figure 1 a-c) Energy band diagrams showing the construction of homogeneous p-n junction and charge transport mechanism under illumination. d) The energy band structure and modulation diagrams of graphene. e) Graphene p-n junction and the plot showing the number of citations against the publication year between 2002 and December 2018, which derived from Web of Science (the retrieves keyword is graphene p-n junctions).

according to the bibliographic as represented in Figure 1e. Preparation of p- and n-type graphene is of particular interest when building the graphene p-n junction. For example, the doping methods applied to graphene include classical interstitial and substitutional doping as well as electronic[63,64] and absorbed[65,66] doping etc., due to the two-dimensional (2D) nature of the material. Although p-type graphene can be fabricated by exposure in air, preparation techniques leading to stable and practical p- and n-type graphene is still highly desirable.

2. Preparation of front-end materials for building the graphene p-n junction

The preparation of front-end materials refers mainly to the fabrication of n- and p-type graphene, which are categorized by the difference in conductivity characteristics. In general, there are two approaches in doping graphene, namely physical (without chemical reaction) and chemical (along with chemical reaction) methods, depending on whether the dopant reacts with graphene due to its exotic physical properties. Electrical doping method has also been explored and demonstrated effective modulation of the Fermi energy of graphene resulting in different conductivity types because of its semi-metal nature. The following sections describe the progress made in the preparation of graphene with p- and n-type conductivity.

2.1. Progress in the preparation of graphene with p-type conductivity

In 2010, Yavari[67] *et al* reported an interesting phenomenon that the conductivity type of graphene changes from intrinsic to p-type and an increase in band gap by 0.029 eV due to absorption of moisture upon exposure to air. The conductivity of graphene is reverted to intrinsic as the water molecules desorb from the surface of graphene by annealing, thus indicating that the entire process is reversible. The absorbed doping method has become one of the most effective modification of the electrical property of graphene due to its high specific surface area (2630 m^2g^{-1})[68]. As graphene is only an atomic layer thick, field-effect transistors based on the material exhibit many excellent characteristics. For example, the Fermi energy of graphene[69] can be tuned by applying a bias voltage resulting in a change in its electronic

property. Such method can lead to electrical doping of graphene. Nevertheless, common approaches that are applied to traditional materials to modulate their electronic characteristics can also be achieved in graphene. Next, methods used to fabricate the graphene with p-type conductivity will be described.

2.1.1 Electrical doping method to prepare graphene with p-type conductivity

Electrical doping method, which produces different electrostatic potential between graphene and electrode through applying a gate voltage to the graphene, tunes the Fermi energy of the graphene by injecting extra charges from the applied electric field.[70] The device structure of field-effect

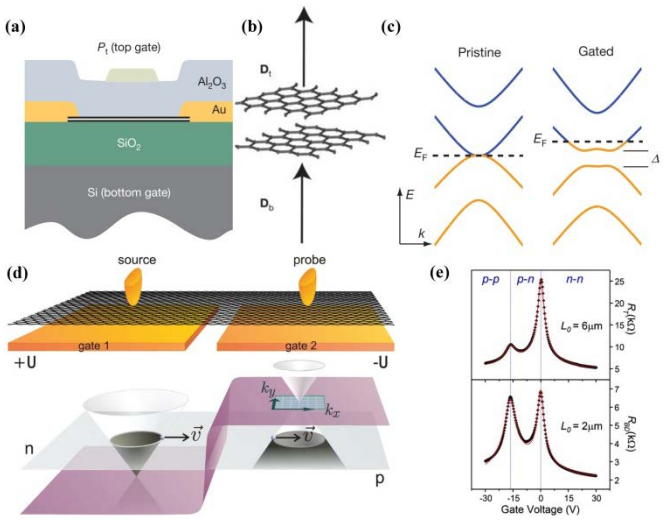

Figure 2 a-c) Schematic diagrams showing double gated FETs based on double-layer graphene as well as energy band structure and Fermi level modulation mechanism of graphene. Reproduced with permission.[42] Copyright 2009, Nature Publishing Group. d) schematic diagram of double gate FETs structure based on single-layer graphene and its electrical modulating mechanism. Reproduced with permission.[63] Copyright 2007, AAAS. e) The conductive type characteristic curve of FETs based on channel materials composed of graphene with different sizes (L_0 = 6 μm and 2 μm) under different gate voltage. The black dots are experimental results, while the red curves are simulation results. Reproduced with permission.[64] Copyright 2007, American Chemical Society.

transistors (FETs) is highly suitable for electrical doping by applying positive and negative bias voltage to modulate the Fermi energy of the graphene between conduction and valence band resulting in the formation of graphene with n- and p-type characteristic,[64] respectively without increase in defect and degree of disorder at the 2D material.

In 2007, double gates FETs based on single-layer graphene was studied by Cheianov[63] *et al* and they reported graphene p-n junction by applying a bias voltage (Figure 2d). Zhang[42] and co-workers studied the electronic structure of graphene by using FET structure, which the channel material is composed of double-layer graphene (as shown in Figure 2a), and revealed the opening of bandgap via the application of the bias voltage. As shown in Figure 2b, an upward electric field occurs under the effect of top-gate voltage D_t and bottom-gate voltage D_b resulting in the following two effects on the double-layer graphene: the modulation of Fermi energy through doping of net charge caused by the difference value D_d ($D_d = D_b - D_t$); the inversion symmetry of double-layer graphene is broken by the average value of D_b and D_t, thus leading to the opening of the bandgap as illustrated in Figure 2c. Chiu[64] *et al* fabricated the FETs based on the single-layer graphene as channel and investigated its electrical properties. They found that the p-type (hole) transport at the channel material can occur at negative drain voltage ($V_D<0$) and gate voltage ($V_G-V_{CNP}<0$, where V_{CNP} is a charge neutral point, namely reference Dirac point), as shown in Figure 2e. A clear distinction between the physics of the electric field tuneable energy gap in few-layer graphene and p-n junctions in single layer graphene can be observed from the above researches. First, the inversion symmetry of few-layer graphene can be broken by electrical doping but single-layer graphene can not be. Besides, the bandgap can be opened for few-layer graphene by this method instead of monolayer due to broking the inversion symmetry. However, the gate-tuneable energy gap, there is a published and well respected review[32] on this topic. Thus, this review need not to state again. As for photonic application, there is a fact that optical and electrical changes are two main considerable factors. The optical properties of graphene which is

modified by electrical doping had been studied by Chang[42] *et al.*. In additionally, most importantly, the more recent first direct measurement of such a gap in electrical transport for graphene which is doped by electrical method had been reported by T. Kohdkov[41] *et al.*. Furthermore, a fact that a small density of defect state appearing at sub-gap energies plays a significant role on electrical transport, making it necessary to produce ultra-clean devices, such this kind of structure which is consist of single-layer graphene with suspended and doubly gated. This energy gap is more readily measured in optical absorption since the small density of defect states does not affect significantly the optical transitions. But a device with a dirty gap is not useful for real life applications, this is why the observation of a clean THz gap in electrical measurement is game changing. Through the research about electrical doping for graphene, an interesting phenomenon that electrical contacts can induce p-n junctions in a single layer graphene had been found by Chiu[64] *et al.*. Although the electrical doping can reversibly control the conductivity and bandgap of graphene without introducing a defect, the structure utilizing this doping method restricts its effective application in the photonic field because of the complex device structure and the need of extra power.

2.1.2 Physical method preparation p-type graphene

Graphene, which is a representative 2D material, has large specific surface area and it provides the possibility of adsorption doping that is reversible and does not involve chemical reaction. The absorbed doping method to prepare p-type graphene is mainly to absorb inorganic molecules, organic molecules, metal films and metal oxides or chloride *etc.* with strong electron trapping capability on the graphene surface as illustrated in Figure 3a. When such dopants are absorbed on the graphene's surface, the Fermi energy level of graphene will shift down the Dirac point leading to graphene with predominantly hole as carriers. When graphene was discovered,[71] it was found

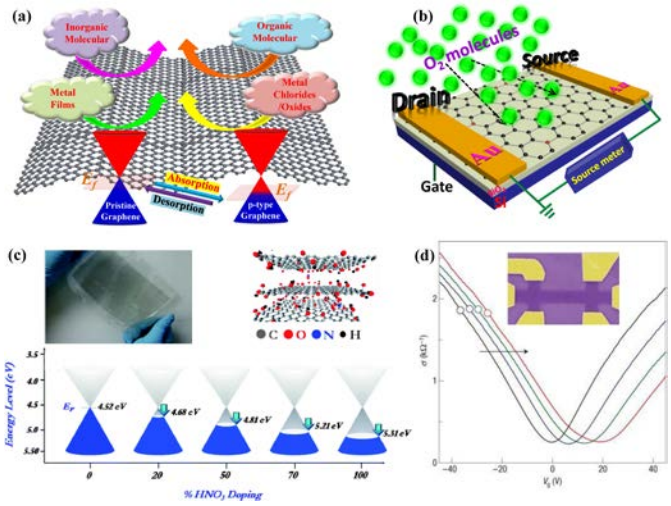

Figure 3 a) Mechanism of adsorption doping on surface of graphene and the main dopants. b) Schematic diagram of oxygen molecules adsorbed on the surface of N-doped graphene. c) Schematic diagram of the HNO_3 doped graphene as well as relationship between concentration and Fermi level. Reproduced with permission.[73] Copyright 2012, The Royal Society of Chemistry. d) Electrical modulation of graphene by adsorption doping with NO_2, inset shows the FETs based on graphene. Reproduced with permission.[65] Copyright 2007, Nature Publishing Group.

that graphene formed p-type conductivity upon adsorption of water molecules in air. It was demonstrated that such adsorption doping of graphene is a reversible process as the graphene is reverted to neutral after several annealing treatments to remove the adsorbed water molecules. To date, inorganic molecules used as dopants on graphene mainly include H_2O, O_2, HNO_3, NO_2, Br_2 and I_2 etc. O_2 is a typical inorganic molecule receptor with strong ability to capture electrons. Chang[72] *et al* fabricated a gas-sensitive field-effect transistor using nitrogen-doped graphene with n- type conductivity as the channel materials as shown in Figure 3b. The transistor was placed in an oxygen atmosphere where electrical testing on the device was performed. The Dirac point of graphene is observed to change from negative to positive when oxygen was continuously

filled and released. In an absence of oxygen, the Dirac point of the graphene is reverted to the original negative position. Such phenomenon suggests that the graphene changes from n-type to p-type conductivity upon adsorbing oxygen and the entire process is reversible. During adsorption doping of O_2, it was also observed that the conductivity of graphene was lower than that of nitrogen-doped graphene, which provides an indication on the O_2 absorption process at the surface of graphene. The mechanism of O_2 molecule adsorbed on the graphene resulting in the transition of the conductive type of graphene can be expressed as:[74]

$O_2(g) \rightarrow O_2(ads)$,

$O_2(ads) + e^- \rightarrow O_2^-(ads)$.

where ads is an abbreviation for the adsorbed dopant. The mechanism explains how absorbed O_2 on the surface of graphene can lead to a change in its conductivity. HNO_3 is another common dopant used for improving the electrical properties and transmittance of carbon materials. It can also modulate the band structure of graphene. Das[73] and co-workers functionalized graphene with different HNO_3 concentrations (e.g. 20, 50, 70 and 100%) on flexible substrate. Its energy band and Fermi energy were studied using ultraviolet photoelectron spectroscopy (UPS). The bottom image of Figure 3c shows the modulation of the energy band and Fermi level of the HNO_3 functionalized graphene film, which was transferred to flexible substrate PET (upper-left image). The upper-right image shows the schematic diagram of graphene doped with HNO_3. The Fermi energy level of the graphene increases from 4.52 eV to 5.31 eV at increasing HNO_3 concentration. The modulation of the Fermi level and increase in hole concentration indicates that the graphene has displayed p-type conductivity. Such phenomenon was also observed in the findings of D'Arsié[75] *et al*. The sheet resistance of graphene is observed to change from 280 Ωsq^{-1} to approximately 125 Ωsq^{-1} after dipping into 63% HNO_3 concentration for 5 minute. Similarly, the resistance of graphene was reported[76,77] to reduce significantly after exposure to NO_2 and the

minimum conductive point moves toward positive gate voltage, which is attributed to hole injection from the NO_2 absorbed on the surface of graphene as presented in Figure 3d. Wehling[78]

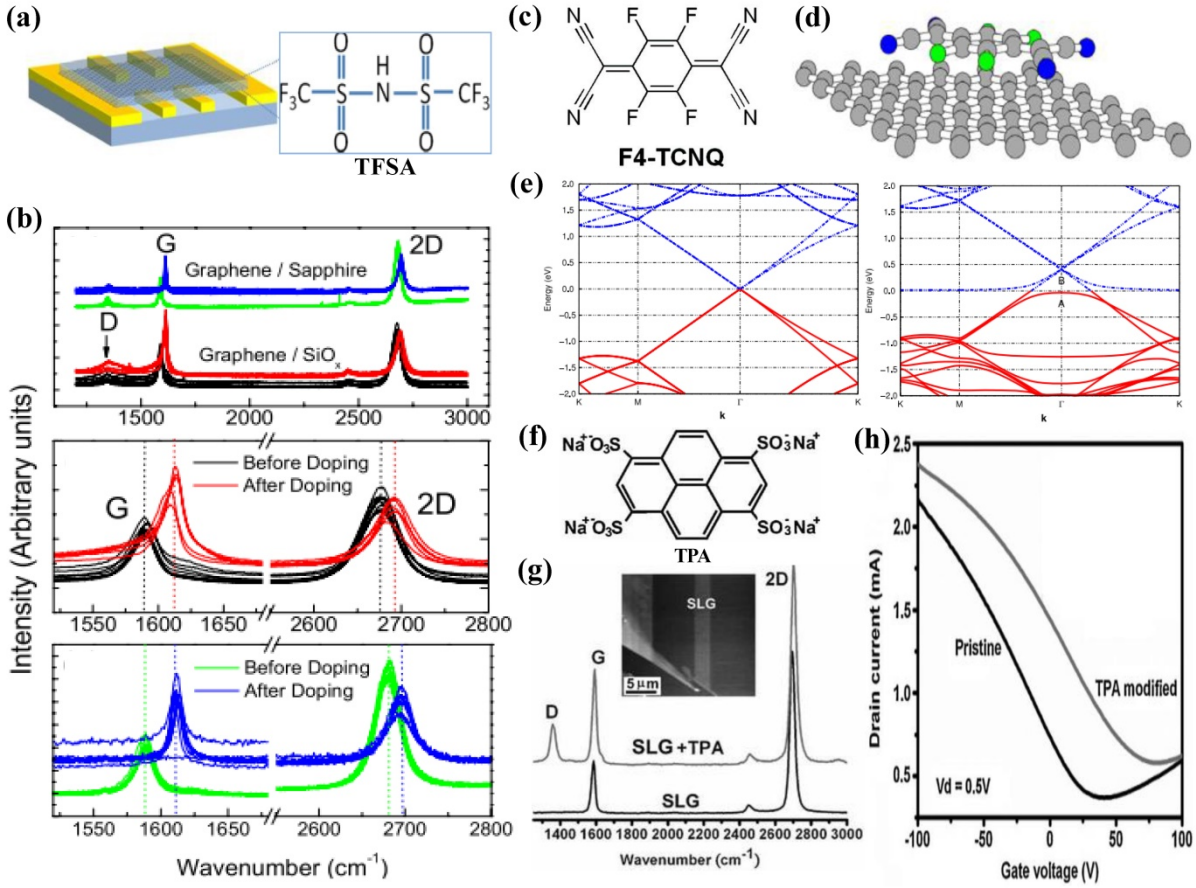

Figure 4 a-b) Schematic diagrams of the structure of FETs based on TFSA organic molecules, inset shows molecular structure of TFSA and its Raman spectral. Reproduced with permission.[80] Copyright 2011, IOP Publishing. c-e) Molecular structure of F_4-TCNQ organic molecules[81] and the energy band structure of graphene and F_4-TCNQ doped graphene. Reproduced with permission.[81,82] Copyright 2007, American Chemical Society and Copyright 2009, IOP Publishing. f-h) Molecular structure diagram of TPA, and its Raman spectra, the electrical characterization results of FETs based on TPA doped graphene. Reproduced with permission.[83] Copyright 2009, Wiley-VCH.

et al reported that the local occupying molecular orbital or Fermi energy level of NO_2 is 0.4 eV lower than the intrinsic graphene Dirac point, thus leading to the formation of p-type graphene. Furthermore, the doping of NO_2 on graphene also results in the capturing of electrons by the dopants. Schedin[65] and co-workers demonstrated that NO_2 gas adsorption doping of graphene is a reversible process. The NO_2 absorbed graphene was annealed at 150 ℃ for two days and subsequent electrical characterization showed that the graphene has reverted to its neutral state. In addition to doping with inorganic molecules as discussed above, Jung[79] *et al* reported the synthesis of graphene doped with Br_2 and I_2, which revealed p-type characteristic as studied using Raman spectroscopy. Although the adsorption doping of inorganic molecule has obvious advantages, such as excellent doping effect and facile method, it can be easily influenced by environment. In contrast, adsorption doping of organic molecule can isolate graphene from the surrounding environment, which is an added advantage. Organic molecule with strong electron trapping capability is used for doping the graphene by absorption to prepare p-type graphene. The absorption results in the transfer of electrons from graphene to the organic molecules. This can be performed by coating graphene with organic molecules dissolved in organic solvents or by utilizing organic molecule evaporation. Double-trifluoromethyl (TFSA) is a well-known p-type organic dopant. Tongay[80] *et al* reported on graphene absorbed with TFSA organic molecule and the doping effect of TFSA investigated by Raman spectroscopy. The fabricated process, which TFSA organic molecules dissolved in nitro-methane solution and coated on the graphene based FETs, is shown in Figure 4a. The top plot of Figure 4b shows the Raman spectra of before and after graphene has been doped on different substrates. The green curve is Raman spectrum of graphene on sapphire substrate and the black curve is from graphene on SiO_x. The Raman spectra show the graphene is of single-layer with relatively small D peak indicating the graphene has very low degree of disorder. The intensity of the D peak has not changed much suggesting that the graphene structure has not been damaged by the absorption doping of TFSA organic molecules.

Enlarged G and 2D peaks are shown in middle plot of Figure 4b. Some observations are made from the Raman spectra after doping, firstly the G (2D) peak shifted from 1588 cm^{-1}(2676 cm^{-1}) to 1611± 2 cm^{-1}(2962±3 cm^{-1}) and secondly the I_{2D}/I_G value reduces from 2.0-2.5 to 0.7-1.0. Such Raman characteristics imply that the graphene has been doped with hole and variation in Fermi level of 0.5-0.7 eV.[84] When doped with TFSA, the sheet resistance of graphene decreases by approximately 70%, the mobility increases by about 63% and the transmittance reduces by about 30-40% in near-infrared wavelength. Tetrafluoro-tetracyanoquinodimethane (F_4-TCNQ) molecule is commonly use as hole buffer layer in the structure of organic light-emitting diodes (OLEDs). [82] It has a strong ability to capture electrons and has a work function of 5.7 eV. Furthermore, it can be easily deposited on a device surface and has a film thickness of 0.2 nm. The molecular structure of F_4-TCNQ is as shown in Figure 4c. The F_4-TCNQ molecule is located in the graphene supercell containing 72 carbon atoms as reported by Pinto[82] and co-workers, as shown in Figure 4d. They simulated the doping effect of the F_4-TCNQ adsorbed on the graphene surface and the energy band structure obtained by theoretical calculation is shown in Figure 4e. While it is worth noting that the p-type graphene is attained via the transfer of electrons from graphene to F_4-TCNQ molecules, another contributing factor is due to the Fermi level of F_4-TCNQ is lower than the Dirac point of graphene. Dong[83] *et al* performed Raman characterization and electrical measurement on single-layer graphene deposited with tetrasodium 1, 3, 6, 8-pyrenetetrasulfonic (TPA) (refer to Figure 4f) dissolved in deionized water. The Raman results show that the D peak is significantly enhanced indicating the surface of graphene was damaged by the absorption doping of TPA organic molecules and the wave number of G and 2D peaks are slightly shifted, as shown in Figure 4g. A prominent doping effect can be justified from the notably decrease in the ratio of $I_{(2D)}/I_{(G)}$ after the adsorption doping of the TPA organic molecule. In order to verify that the TPA doping is hole doping, FETs based on pure graphene and graphene doped with TPA were characterized by electrical measurement. It was found that the lowest resistance point of the pure

single-layer graphene is located at around +30 V of the gate voltage due to the fact that the graphene is exposed to air leading to the adsorption of inorganic molecules, such as water vapor and oxygen. By contrast, the lowest resistance point of single-layer graphene doped with TPA is situated at approximately +80 V, which is shifted about +50 V from the pure graphene. This indicates that the doping of TPA leads to hole doping and reduces the electron concentration at the single-layer graphene. In addition to the doping of the above-mentioned organic molecules, other organic molecules exhibiting strong electron trapping capabilities are also used as p-type dopant in graphene. For example, Lu[85] *et al* simulated the doping of tetracyanoethylene (TCNE) organic molecules for graphene and obtained several stable adsorption mode as well as effective modulation of the bandgap and conductive type of the single and double-layer graphene. There are other molecules[86,87] that can be used as absorption dopants as previously studied by some groups. Indeed organic molecule doping has obvious doping effect and can effectively regulate the electrical properties of graphene, but there are some stability issues when using organic molecule especially at high temperature. Many organic molecules are extremely unstable and volatile under high temperature, which leads to a significant decrease in doping effect. During the preparation of p-n junction, high temperature annealing is often required for the formation of the junction. Hence, the annealing process will limit the application of absorption doping of organic molecules in p-n junction. Apart from adsorption doping of inorganic and organic molecules, metals with strong electron trapping capability when adsorbed on the surface of graphene can also be used as p-type dopants. The metal atoms are deposited onto the graphene surface through heat evaporation. The adsorption doping mechanism of metal atoms on graphene was studied by Giovannetti[88] *et al* using DFT calculations. The absorption doping effect of Ni, Co, Pd, Al, Ag, Cu, Au and Pt on graphene, and the work function of each metal and graphene are listed in Table 1. It was found that the contact distance between metal atoms and graphene has a significant impact on the doping effect of graphene, and the influence of contact on the doping effect is

illustrated in Figure 5a. A potential difference (ΔV) is introduced as the metal (having a work function, W_M) is in contact with the graphene resulting in the uniformity of the Fermi level across the two materials. The work function of graphene is W_G, when it is not in contact with metal. After

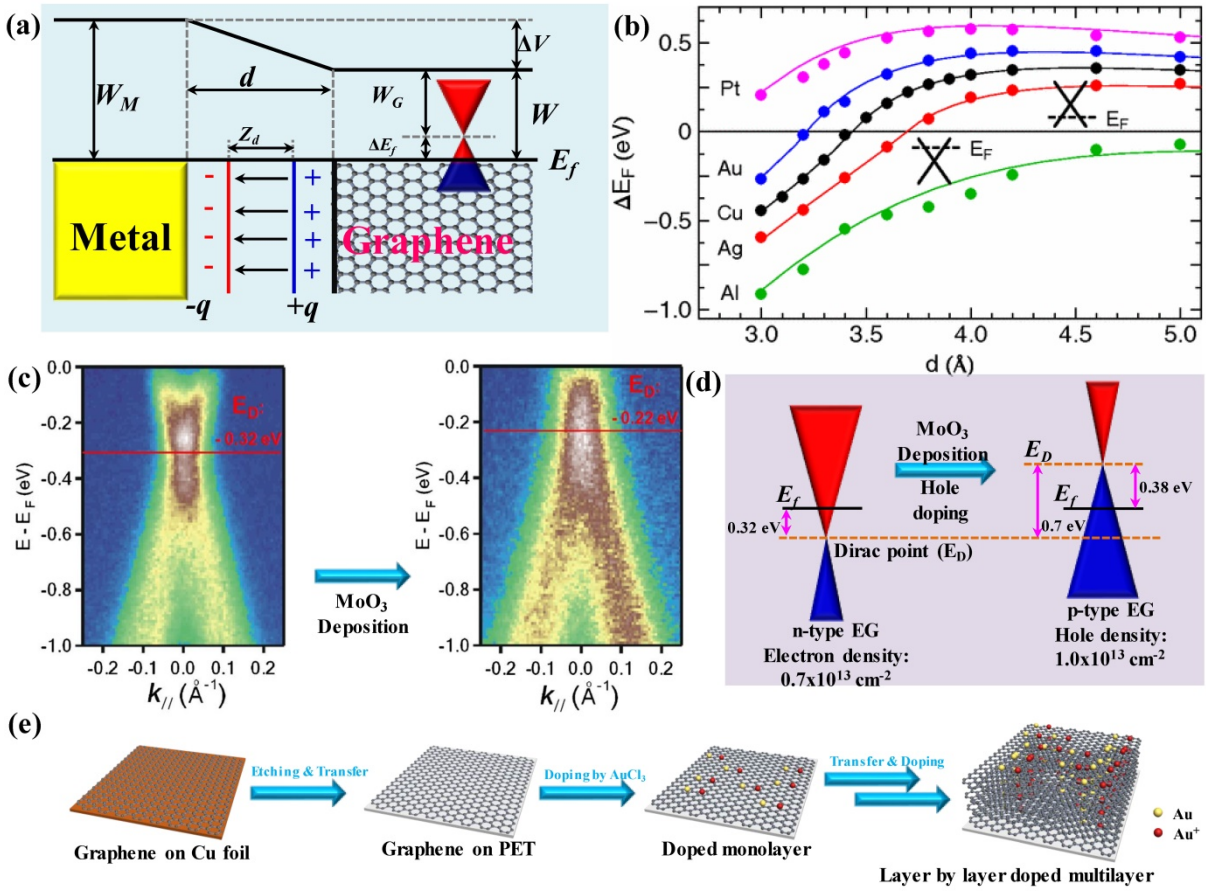

Figure 5 a-b) Schematic diagram showing the doping mechanism of each metal atom and the modulation of Fermi energy level, and also the distance between the graphene and metal film. Reproduced with permission.[88] Copyright 2008, The American Physical Society. c-d) The ARPES results of graphene before and after doping with MoO_3 and schematic diagram of the Fermi level modulation. Reproduced with permission.[89] Copyright 2010, AIP Publishing. e) Schematic diagram showing the preparation of graphene doped with $AuCl_3$ via LBL. Reproduced with permission.[90] Copyright 2010, American Chemical Society.

the metal is in contact with graphene, its work function becomes $W = W_M - \Delta V$, hence resulting in the modulation of the Fermi level of graphene $\Delta E_f = W - W_G$. Since ΔV depends on the contact distance (d) between metal and graphene, the modulation of the graphene Fermi energy level is

Table 1 The work function of metal (W_M) and graphene doped with metal (W) under equivalent distance of the surface d_{eq} between graphene and metal based on panel (111) by calculation. Reproduced with permission.[91] Copyright 1997, IOP Publishing.

Co	Gr	Ni	Co	Pd	Al	Ag	Cu	Au	Pt
d_{eq} (Å)	—	2.05	2.05	2.30	3.41	3.33	3.26	3.31	3.30
W_M(eV)	—	5.47	5.44	5.67	4.22	4.92	5.22	5.54	6.13
W(eV)	4.48	3.66	3.78	4.03	4.04	4.24	4.40	4.74	4.87

related to the contact distance. Therefore the electrical regulation of graphene by metal adsorption doping is not only directly related to the work function of the metal, but also to the contact distance between the metal and the graphene, as shown in Figure 5b. As can be seen from the diagram, when the metal work function is higher than that of the graphene (0.9 eV), the p-type doping effect on graphene will occur. The conductivity type of graphene can be changed from n-type to p-type when the contact distance increases, but some metals, such as Al[92], with low work function will only result in a decrease of the doping effect instead of a change in the conductivity type of graphene. P-type doping can also be achieved by depositing metal oxides, such as MoO_3 and ReO_3 (work function ~6.8 eV)[93] etc., on the surface of graphene. Chen[90] *et al* deposited a MoO_3 (work function ~6.8 eV) film on graphene prepared by SiC epitaxial growth and its electrical properties were studied. The band structure of graphene before and after doping was investigated by angle-resolved light emission spectra (ARPES), as shown in Figure 5c. The Fermi level of a bilayer graphene prepared by SiC epitaxial growth is 0.32 eV above the Dirac point and thus indicating n-type graphene. After the deposition of MoO_3 at a thickness of 0.2 nm, the Dirac point of the graphene is apparently shifted above the Fermi level as illustrated in Figure 5d. After

depositing 0.8 nm of MoO_3, electrons at the graphene are transferred out of the surface resulting in p-type graphene. Therefore p-type is formed when the modulation band of graphene moves 0.7 eV upward relative to the Fermi energy level, in other words the Fermi level moves 0.38 eV under the Dirac point. By simulation, the reported electron concentration of epitaxial-grown double-layer graphene is 0.7 $\times 10^{13}$ cm^{-2} and the hole concentration is about 1.0 $\times$ 10^{13} cm^{-2} after doping. Such results suggest that the graphene can be effectively p-type doped by depositing MoO_3 film on it. Xie's[94] research group also confirmed the p-type doping effect of MoO_3 and measured the mobility of graphene which decreases from 8700 $cm^2V^{-1}s^{-1}$/7300 $cm^2V^{-1}s^{-1}$ to 7300 $cm^2V^{-1}s^{-1}$/6150 $cm^2V^{-1}s^{-1}$ after the deposition of MoO_3. In addition, metal chlorides, such as $AuCl_3$,[90,95,96] $NbCl_5$,[97] $FeCl_3$,[98-102] and $RhCl_3$[103] etc., can also be considered as p-type dopants for graphene. Gunes[90] and co-workers doped graphene with $AuCl_3$ (work function ~5.6 eV)[104] via two methods, namely layer-by-layer stacking and top-depositing, and the former demonstrated better doping effect. It was found that the position of the G peak in Raman spectra shows the characteristics of p-type doping. The up-shifting of the G peak position is due to phonon curing effect as a result of charge extraction.[105,106] The layer by layer doping process is illustrated in Figure 5e. Meng[97] and co-workers prepared $NbCl_5$ doped graphene and reported a reduction in the charge mobility from 180 $cm^2V^{-1}s^{-1}$ to 85 $cm^2V^{-1}s^{-1}$, revealing dominance of hole conductivity with its carrier concentration increases by two orders of magnitude. Besides, same doping method, layer-by-layer stacking, had been carried out for $FeCl_3$ (work function ~5.2 eV) doping graphene by many research groups[98-101]. All the works demonstrate that $FeCl_3$ doping graphene is effective to gain p-type graphene and remains stable in hostile environment.

Previous studies have demonstrated the effective regulation of Fermi energy level of graphene by the adsorption doping. The surface adsorption of inorganic molecules is extremely unstable and the graphene cannot be isolated from the surrounding environment. While doping with organic molecules can effectively shield graphene from the surrounding environment, the application of

the doped graphene is limited by the instability of the organic molecules. By depositing metal film or metal oxide/chloride on the graphene surface, it is possible to address the high temperature instability of doping and to shield the graphene from the surrounding environment. Such doping

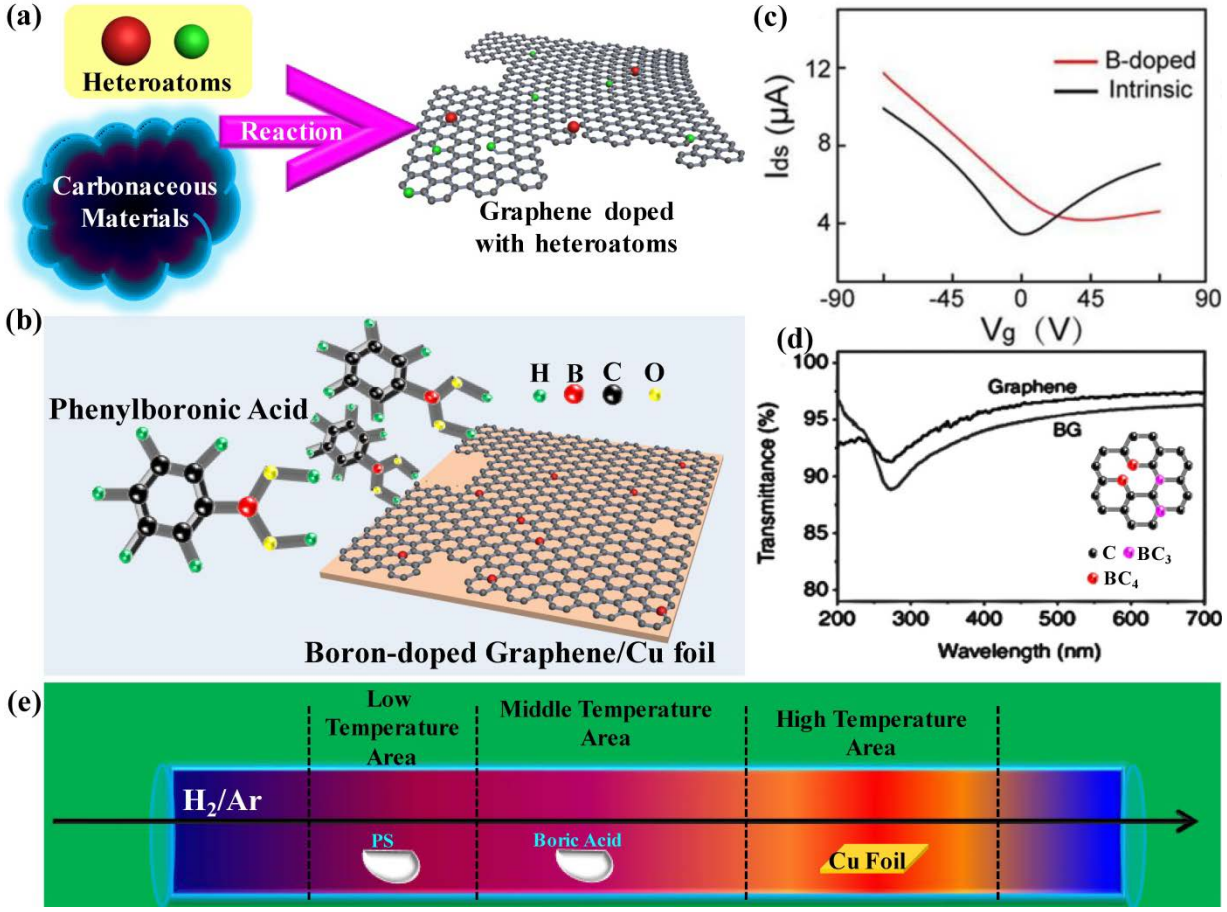

Figure 6 a) Schematic diagram of doped graphene prepared by chemical method; b-c) Electrical measurement results of FETs based on channel materials composed of B-doped graphene prepared by phenylboronic acid, in which the green balls are H atoms, red balls for B atoms, black balls for C atoms, yellow ball as O atoms. Reproduced with permission.[105] Copyright 2013, Wiley-VCH. d) Optical characterization of B-doped graphene films, inset shows the chemical bonding structures of B atoms doping. Reproduced with permission.[106] Copyright 2012, Wiley-VCH. e) Schematic diagram showing the preparation of B-doped graphene by using polystyrene as carbon source and boric acid as B source via CVD method. Reproduced with permission.[107] Copyright 2012, The Royal Society of Chemistry.

method is indeed worthy of consideration. However, the metal doping is limited by the contact distance, which makes effective doping of graphene a technical challenge. Thus, some technical requirements for the construction of graphene homogeneous p-n junction are presented at the later stage.

2.1.3 Chemical method preparation of p-type graphene

Chemical method, which primarily involves chemical reaction to produce new materials, has been used to prepare doped graphene through reaction between carbonaceous materials (e.g. consisting of carbon-containing inorganic molecules, organic molecules and graphene) and p-type dopant atoms, as shown in Figure 6a. The heterogeneous atoms doped graphene can be by means of substitution (when the dopant atomic size is close to that of carbon atom, such as B atom) and interstitial (when the atomic size is far larger or smaller than that of carbon atom, such as S atom) doping. Chemical vapor deposition (CVD) and plasma deposition are the two main methods used to prepare doped graphene. The CVD method can be divided into solid chemical vapor deposition, liquid chemical vapor deposition and gas chemical vapor deposition, according to the different phase state of precursor. As shown in Figure 6b, Wang[105] and co-workers coated a copper foil with phenylboronic acid, which is used as carbon and B source, was annealed at high temperature to prepare boron-doped graphene via pyrolysis. The B-doped graphene is used as the channel material of FETs and its electrical characteristics are as shown in Figure 6c. The plot shows the minimum resistance point of the B-doped graphene FET is situated at the positive gate voltage, hence indicating the formation of p-type doping characteristics. The results imply that B atoms have notably doping effects on graphene and the calculated charge mobility of the doped graphene is approximately 800 $cm^2V^{-1}s^{-1}$ at room temperature. The above-mentioned methods in general utilize carbon-containing materials and heteroatoms-containing materials for pyrolysis and deposition under high temperature. Wu[107] *et al* prepared B-doped graphene using a CVD

process involving different temperature stages, for example, polystyrene (as carbon source), boric acid (as B source) and copper foil (as substrate) were placed at low-temperature (150℃ - 300℃), medium-temperature (450℃ - 550℃) and high-temperature (1000℃) areas, respectively with a flow of H_2 and Ar as shown in Figure 6e. Firstly, polystyrene and boric acid transform to gaseous materials at a certain temperature and then driven by a gas mixture of H_2 and Ar. Secondly, the two gaseous phase materials are decomposed and deposited at the surface of copper foil at high temperature. Finally, the graphene films doped with B are grown by the metal Cu catalysis. Electrical measurements were performed on the B-doped graphene based FETs and found that the Dirac point of the doped graphene is located at the positive gate voltage, thus implying p-type characteristics with charge mobility at 450 - 460 $cm^2V^{-1}s^{-1}$.

B ($2s^22p^1$) atom is substituted into the graphene and is adjacent to a carbon atom. It has one valence electron less than carbon atom. Due to the fact that B itself lacks an electron and the bonding length of B-C (approximately 1.50 Å) is larger than the bonding length of C-C in the intrinsic graphene (1.40 - 1.42 Å), B-doping therefore results in p-type characteristic and slight modification in lattice parameters.[108-110] Rani[108] *et al* performed DFT theory calculations and showed that the energy gap of the graphene is opened by 0.14 eV due to B doping. Two predominant types of B atomic bonding structures in the lattice of doped graphene prepared by CVD method are observed, such as Boron silane (BC_4) and graphite Boron (BC_3),[106] as illustrated in inset of Figure 6d. Compared to the more common BC_3 bonding (B replaces the C in the hexagonal carbon lattice), BC_4 is derived from marginal or excessive defects resulting in structural damage, which will dramatically change the properties of graphene. The doped graphene films can be prepared by using liquid precursor as both a carbon source and a doping source. For example, Li[106] *et al* directly dissolved boron powder (as B source) in ethanol solution (as carbon source), B-doped graphene was synthesized by catalyzing the mixture with Cu at 1000 ℃. The transmissivity of B-doped graphene films can be observed at a range between 250

nm and 700 nm, and its transmittance reduces significantly after B doping, which indicates improvement in the absorption of B-doped graphene as shown in Figure 6d. Dopant atoms with a large difference in size from carbon atoms are effectively doped in the form of interstitial doping instead of substitution. An example of such dopant is sulfur atom. Gao[111] and co-workers prepared S-doped graphene via CVD method by using liquid organics (e.g. S powder dissolved in hexane) as precursor and the whole process curve is shown in Figure 7g. The S-doped graphene films were characterized by transmission electron microscopy (TEM), which shows black spots

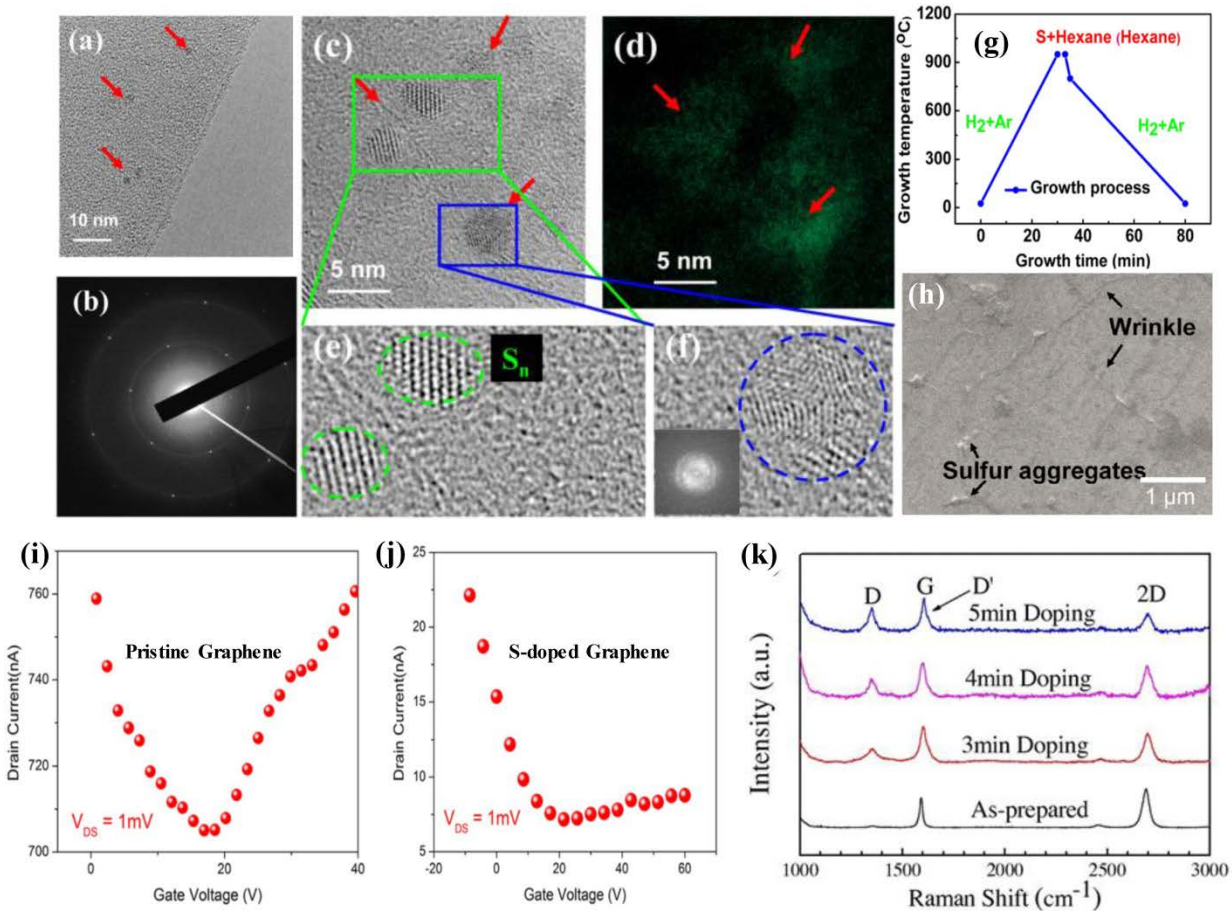

Figure 7 a-f) TEM and selective electron diffraction (SAED) images of S doped graphene films. g) Graph showing the preparation process of S doped graphene via CVD routine. h) Scanning electron microscopy image of S-doped graphene. i-j) Electrical measurement results of FETs based on intrinsic graphene and graphene doped with S. Reproduced with permission.[111]

Copyright 2012, IOP Publishing. k) Raman spectra of S-doped graphene films with different H_2S gas exposure durations. Reproduced with permission.[112] Copyright 2014, Elsevier.

representing S elements on the surface of graphene as shown in Figure 7a-f. From the selective area electron diffraction (SAED) patterns, it reveals that the crystal lattice of graphene is not seriously damaged and the sulfur atoms exist in graphene in the form of interstitial doping. Scanning electron microscopy (SEM) image indicates that sulfur aggregation is present on the surface of the graphene film as shown in Figure 7h. An advantage on the use of the liquid precursor source is its short deposition time of about 2.5 min, hence making the preparation process of doped graphene highly efficient. The FETs with channel material comprised of S-doped graphene was fabricated and studied. It was found that the Dirac point of the S-doped graphene is located at positive gate voltage as presented in Figure 7j. By comparing the electrical measurement results with the intrinsic graphene, it can be seen that the electrical symmetry of the S-doped graphene has been damaged. It is worth noting that the Dirac point of the intrinsic graphene is located at the positive gate voltage because the graphene has been exposed to air and adsorbed with molecules, such as water vapor (Figure 7i). The calculated charge mobility is about 90 $cm^2V^{-1}S^{-1}$, which is much lower than the charge mobility of the intrinsic graphene. This can be attributed to defects in the S-doped graphene. Apart from the use of liquid precursor to prepare doped graphene films, Liang[112] *et al* prepared S-doped graphene films by using vapor method, which the graphene film was doped in the quartz tube under the atmosphere of H_2S at 1000°C. TEM characterization shows that the S element also appears as black spots, which has similar observation as the former technique. It was found that the D peak (e.g. defect peak) intensity at the Raman spectra increases as the duration of H_2S increases, as shown in Figure 7k. This indicates that there is damage to the lattice of graphene upon doping with S atoms. Electrical measurements performed on the doped graphene shows p-type characteristics with charge mobility of about 68 $cm^2V^{-1}s^{-1}$. The p-type behavior of S-doped graphene is due to the interstitial

doping of S atom instead of substitution doping as reported for S-doped diamond films. The S-doped diamond films exhibit n-type characteristic because the S atoms substitute the carbon atoms, which result in S atom releasing two free electrons and form a stable electronic structure. Instead, S atoms are interstitially doped in graphene as studied using TEM and the S atom can reach a balanced state by capturing two free electrons, hence the S-doped graphene exhibits p-type behavior. However, n-type doping effect has been observed from S-doped graphene prepared by pyrolysis of H_2S gas as studied using Raman and FETs measurements performed by Choi[113] *et al.* Apart from the CVD methods described above, currently the most common and effective

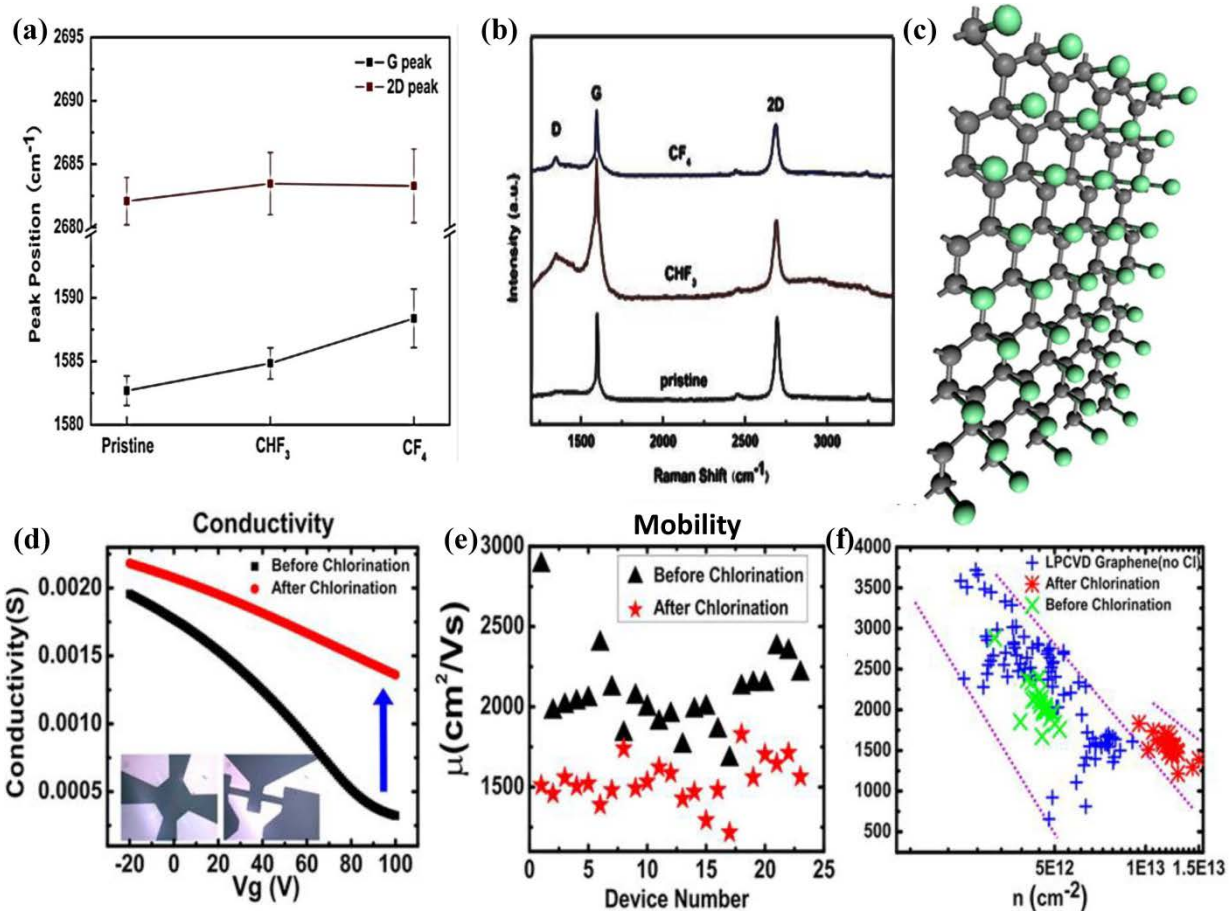

Figure 8 a-b) Raman spectra of F plasma-doped graphene films. Reproduced with permission.[114] Copyright 2012, IOP Publishing. c-f) Structural diagram of Cl plasma-doped graphene and its electrical measurement results. Reproduced with permission.[115] Copyright 2013, American Chemical Society.

method is the plasma method. Plasma is commonly used in device surface cleaning. It is formed by ionization of gas and is often used for surface bombardment to improve surface properties of material. Due to the high specific surface area of graphene, plasma treatment of the surface can effectively dope graphene with plasma gas molecules via surface chemical reaction, thereby changing the electrical properties of graphene. Chen[114] and co-workers treated graphene film with plasma in CHF_3 or CF_4 environment to dope the graphene with F. Raman spectroscopy technique is an effective method in determining the doping type of graphene. The dynamic effect of carrier group will lead to enhancement in the G peak vibration of the graphene as a result of departure of the carrier group in equal enthalpy ground state.[84,116,117] Consequently, the position of G and 2D peaks shift up when the doped graphene is p-type, and shift in the opposite direction if doped n-type.[83] Moreover, the ratio of $I_{(2D)}/I_{(G)}$ for graphene doped with p-type dopants could reduce significantly.[118] Studies performed using Raman spectroscopy technique verify the formation of p-doped graphene by CHF_3 or CF_4 plasma doping as shown in Figure 8a. The Raman results of a single-layer graphene treated with plasma of CHF_3 or CF_4 indicate the introduction of defect on the graphene upon doping with F as presented in Figure 8b. Furthermore, the lattice defect of CHF_3 plasma-treated graphene is larger than that of CF_4, hence suggesting that the CF_4 is a better choice than CHF_3 for F-doped graphene by plasma treatment. Zhong[119] and co-worker prepared F-doped graphene by using SF_6 plasma treatment and fabricated high performance graphene/silicon solar cells with conversion efficiency of up to 13.38%. Similarly, Cl-doped graphene can also be prepared by plasma treatment method. For instance, Zhang[115] *et al* successfully prepared Cl-doped graphene containing up to 45.3% of Cl element by placing graphene in a plasma of Cl (close to C_2Cl and its structural diagram is shown in Figure 8c). The doped graphene is stable for more than a week in air. Hall measurements on the Cl-doped

graphene reveal p-type carrier conductivity and charge mobility is as high as 1535 $cm^2V^{-1}s^{-1}$, which is considerably higher than that of the chemically doped graphene but still lower than that

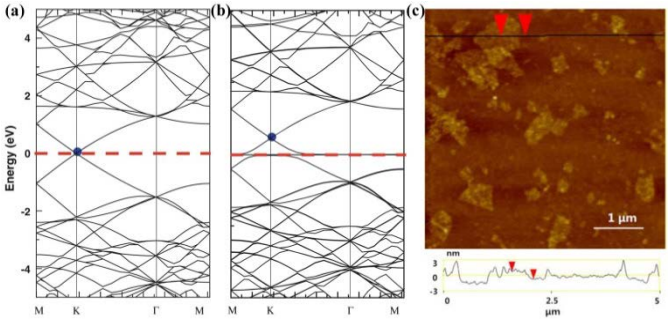

Figure 9 a-b) The variation on energy band structure of I-doped graphene via DFT theoretical calculation. c) Atomic force microscopy (AFM) image of I-doped graphene oxide films, the bottom line profile shows the film thickness measurements between the two red arrow at the above image. Reproduced with permission.[120] Copyright 2013, Springer.

of the intrinsic graphene, as shown in Figure 8e. It is believed to be caused by defect formation due to ion bond of chlorine and covalent bond of carbon. As shown in Figure 8d, electrical measurements performed on a FET based on the Cl-doped graphene as a channel material reveal a reduction in the sheet resistance of the graphene from 678 Ωsq^{-1} to 342 Ωsq^{-1}.The study also found that the mobility of the Cl-doped graphene decreases as the charge concentration increases as shown Figure 8f. It is worth noting that the decrease in mobility is more significant for plasma treatment method than that prepared by CVD, and decreases more, as compared to the Cl plasma treatment, as shown Figure 8f. The use of plasma method in doping graphene with heterogeneous atoms is to ensure the conductive type modulation of graphene, minimize lattice damage and maximize charge mobility of graphene. In addition, Wang[120] *et al* prepared p-type graphene with iodine doping on graphene oxide, as shown in Figure 9c. DFT theoretical calculations show that the I atom is substitutionally doped into graphene modulating its Fermi level under the Dirac point, hence converting the graphene to p-type conductivity as shown in the plots of Figure 9a,b.

Thermal doping methods have also been explored. Wang[121] *et al* fabricated B-doped graphene by thermally exfoliation of graphene oxide in BF_3 atmosphere and its carrier concentration can be controlled by different temperatures. Besides, Zhu[122] *et al* successfully synthesized B-doped graphene with p-type conductivity by using solvent thermal method. Various heterogeneous atoms doped graphene and doping methods have been widely studied. The doping effect of the various doped graphene is studied according to the different applications. However, further investigation on the conductivity type of the various doped graphene is still needed. To prepare p-n junction for application in the photonic field, it is necessary to study the conductivity type and carrier concentration of the doped-graphene. Such studies will reveal the doping mechanism of heterogeneous atom doped graphene. In term of the preparation method, the present chemical doping method still requires further development. As compared to the physical doping method, the chemical doping method is more effective, stable and controllable. However, the chemical method can lead to defects and reduction of graphene-related photoelectron properties, which present major issues during application and therefore require much attention.

2.1.4 Other methods for preparing p-type graphene

In addition to the electrical, physical and chemical methods, there are other novel methods in doping graphene, such as photon-induced doping and substrate heterogeneous atom doping methods. Wang[123] *et al* prepared graphene/n-silicon heterostructures and performed Raman measurements during incidence of white light on the surface. They found that the graphene G peak and 2D peak position are shifted when the light is turned on and reverted back after the light is turned off. The shift of both G and 2D peaks position is attributed to charge doping based on previous research findings.[84,126] For example, the G and 2D peaks of the graphene would shift up when it is doped with holes and shift down due to stress effect. The Raman results demonstrate the doping effect of white light on graphene by lowering its Fermi level to below the Dirac point,

which leads to p-type doping. This interesting phenomenon is attributed to the light, the electron-hole pairs produced by the electric field at the Schottky junction, the electrons at the edge of silicon aggregation, and the hole at the defects of graphene gathered at the edge of graphene, hence resulting in the Fermi level of the graphene to position below the Dirac point. Such phenomenon is attributable mainly to this particular structure and the specific doping mechanism is illustrated in Figure 10a. In additionally, the fact that introduction of light can shift down the Fermi level of graphene had been demonstrated by Jones[125] et al, as shown in Figure 10f. Through the generation of carrier in the organic material under the illumination, the photo-induced pairs can inject into graphene via control the gate voltage for modifying the conduction type of graphene. By this method, p-type graphene had been obtained.

Goncher[52] *et al* realized locally p- or n-type doped graphene on mica substrate by controlling the level of the substrate. P-type doped graphene is observed around a water nucleation spot originated from beneath the substrate, while n-type doped graphene is observed from K^+ ion trapped interfacial area, as illustrated in Figure 10b. Scanning tunneling spectroscopy (STS) measurement was performed and showed local doping of n- and p-type on the exfoliated graphene on mica sheet. Localized doping is attributed to the fact that substrate can regulate the local area of electrons and holes at the nanoscale level, as shown in Figure 10c. The modulation of the substrate for doping graphene with a certain conductivity type is an important method. The energy band modulation of graphene was studied by transferring a layer of graphene on a boron-doped silicon wafer as performed by Diana[124] *et al*. The study found that annealing at a temperature of 400 K resulted in the diffusion of B in silicon to the graphene hence doping graphene with B atoms (Figure 10d). Furthermore, this results in the opening of the graphene bandgap by 0.2 eV and causes its Fermi level to modulate below the Dirac point, thus resulting in p-type conductivity. In the case of B-doped graphene, the single and double vacancies are produced in graphene, as shown in Figure 10e. This is determined by the heterogeneous atoms of the substrate, which are

introduced to the graphene due to external effects on the substrates, resulting in a change on the conductivity type of the graphene.

In conclusion, the electrical, physical, chemical and other methods in doping graphene have demonstrated their ability to tune the electrical properties of the 2D material. The electrical doping has not led to structural damage on graphene and has maintained its excellent electrical characteristic. As electrical modulation requires complex structures, this doping method is unsuitable for the construction of graphene p-n junction and its application in the field of optoelectronics. The physical doping method involves the adsorption of dopants at the graphene, which exhibit a high specific surface area.

The electron transfer between the adsorbed dopants and graphene result in the formation of p-type graphene. However, the instability and lack of ability to control the doping effect of the absorbed dopants are hampering the construction of the graphene p-n junction. Preparation of p-type

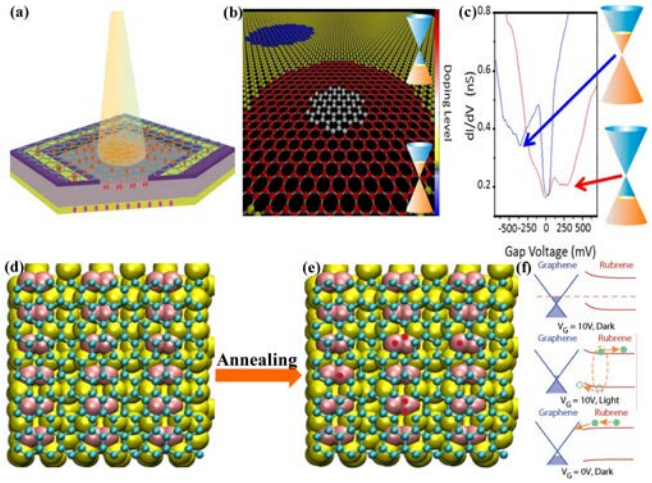

Figure 10 a) Schematic diagram on the preparation of doped graphene by optical method. Reproduced with permission.[123] Copyright 2014, American Chemical Society. b-c) Schematic diagram of the conductive type of graphene controlled by the horizontal nanometer level of substrate and plot of STS measurement. Reproduced with permission.[52] Copyright 2013, American Chemical Society. d-e) Illustration of boron-doped graphene coated on silicon with plane (100), which is introduced by annealing, the red dot in the figure (e) represents single and double holes introduced by doping B. Reproduced with permission.[124] Copyright 2017, IOP Publishing. f) Schematic the conductive type of graphene controlled by the light. Reproduced with permission.[125] Copyright 2017, Wiley-VCH.

graphene via chemical doping method is mainly through the displacement of heterogeneous atoms resulting in a change of the electrochemical properties of graphene by interstitial doping. The introduced heterogeneous atoms by the chemical doping method can destruct the graphene lattice. Such defects have detrimental effects on the electrical properties of graphene, hence impeding the development of high performance optoelectronic devices based on the doped-graphene. There are other new doping methods, which the doping mechanism is not yet fully understood, and they require further studies prior to using them in the construction of the graphene p-n junction. All of these methods have its pros and cons, thus careful consideration is required when choosing an appropriate doping method in the construction of the graphene p-n junction.

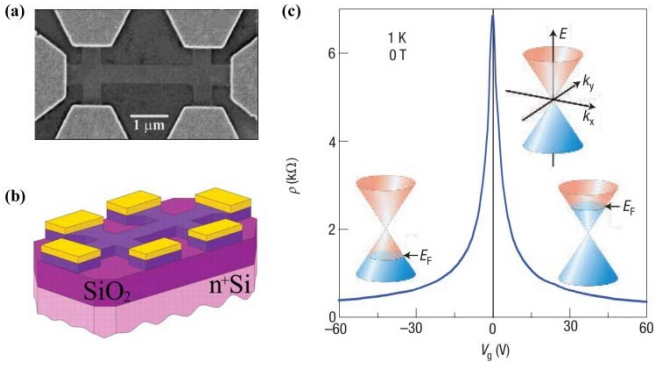

Figure 11 a) SEM image of FET based on graphene. b) Schematic diagram of the FET based on graphene. Reproduced with permission.[71] Copyright 2004, AAAS. c) The electrical measurement results of the FET based on graphene under bias, inset shows the schematic diagram of graphene conductive type modulation. Reproduced with permission.[127] Copyright 2007, Nature Publishing Group.

2.2. The progress in the preparation of n-type graphene

Similar to the preparation of the p-type graphene, the methods for preparing the n-type graphene can also be divided into electrical, physical, chemical and other methods. The difference is that n-type graphene is produced mainly by injecting electrons, such as applying a positive gate voltage or using donor materials as a doping agent, during its preparation. As graphene exhibits p-type conductivity upon exposure to air due to the absorption of oxygen and water vapor, it is therefore more difficult to prepare graphene with n-type conductivity that is stable in air. Such development is particularly of great interest and demand.

2.2.1 Electrical method to prepare n-type graphene

The electrical method to prepare n-type graphene is similar to that of p-type graphene. It involves the injection of electrons at the gate by applying positive gate voltage causing the Fermi-level to modulate, hence forming n-type graphene, as illustrated in Figure 11. The mechanism for the electrical conductivity of graphene is similar to section 2.1, therefore it is not discussed here.

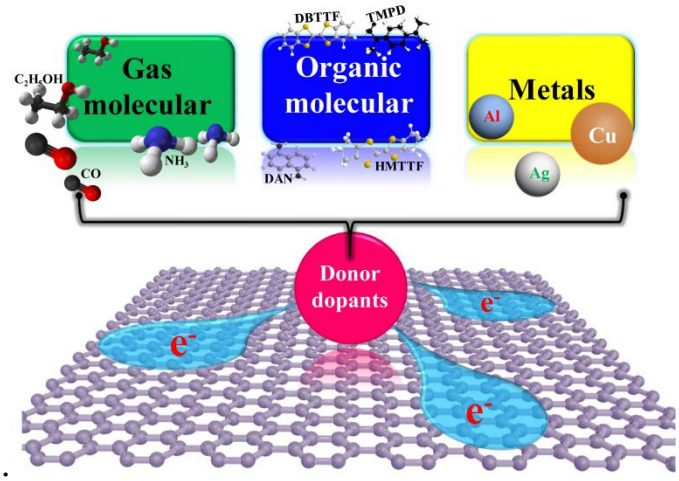

Figure 12 Schematic diagram illustrating the preparation of n-type graphene by physical methods.

2.2.2 Physical method to prepare n-type graphene

Due to the high specific surface area of graphene, it can easily adsorb donor dopants, such as inorganic gas molecules (ethanol, NH_3 and CO)[65], organic molecules(dibenzotetrathiafulvalene(DBTTF), N,N,N',N'-tetramethyl-pphenylenediamine (TMPD), 1,5-diaminonaphthalene (DAN), hexamethyltetrathiafulvalene (HMTTF)[128] and metals (Al , Ag , Cu[88] *etc.*). The physical method to prepare n-type graphene is mainly via physical adsorption of the donor dopants at the graphene surface causing a transfer of electrons from the dopants to the graphene as depicted in the schematic diagram of Figure 12. This result in shifting of the Fermi level to above the Dirac point of graphene, thus forming n-type conductivity.

In 2009, Dai[129] *et al* developed a FET, consisting of graphene nano-ribbon with width of 30 nm as channel material (as shown in Figure 13c), which was thermally annealed in an atmosphere of ammonia, as illustrated in Figure 13a. Comparing the measurements of the FETs based on the differently treated graphene as channel materials, such as graphene in air and annealed in ammonia atmosphere, it can be seen that the Dirac point of graphene in air is situated at the positive gate voltage indicating weak p-type graphene. However, the Dirac point of graphene

annealed in the ammonia atmosphere is situated at gate voltage of -30 V, implying that the Fermi level of the graphene is significantly modulated and the graphene exhibits n-type conductivity as shown in Figure 13b. In order to demonstrate this phenomenon is caused by the absorption of ammonia at the surface of graphene after annealing in the ammonia atmosphere, X-ray photoelectron spectroscopy (XPS) study was performed to characterize its surface. The XPS characterization results show the presence of N 1s peak at the surface of graphene annealed in the ammonia environment. These nitrogen atoms are mainly absorbed at the edge of graphene due to the instability of the suspension bond and hence ammonia molecules are readily absorbed at the edge as illustrated in Figure 13d. Even though the graphene was annealed in the ammonia atmosphere, its internal structure has not been damaged as the ammonia molecules are mainly adsorbed at the edge of graphene. Hence, the charge mobility of graphene remains high. However,

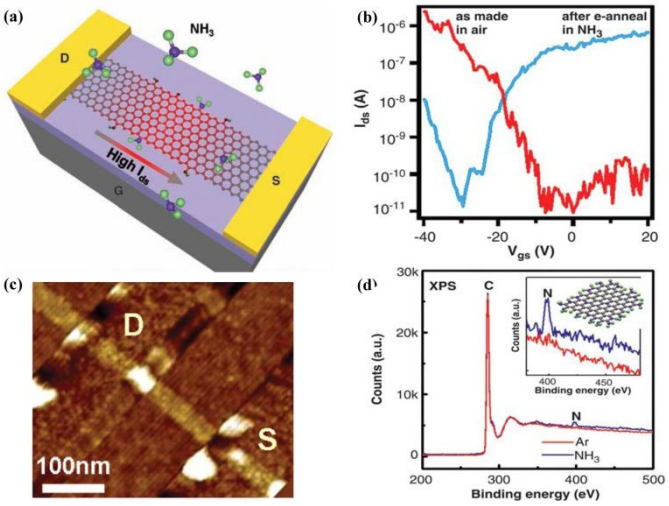

Figure 13 a) Schematic diagram of FET based on graphene annealed in ammonia atmosphere. b) The electrical measurement results of the FET based on graphene annealed under ammonia atmosphere and exposed to air. c) SEM image of the FET based on graphene nano-ribbon. d) X-ray photoelectron spectroscopy of graphene annealed under ammonia atmosphere with argon protection. Reproduced with permission.[129] Copyright 2009, AAAS.

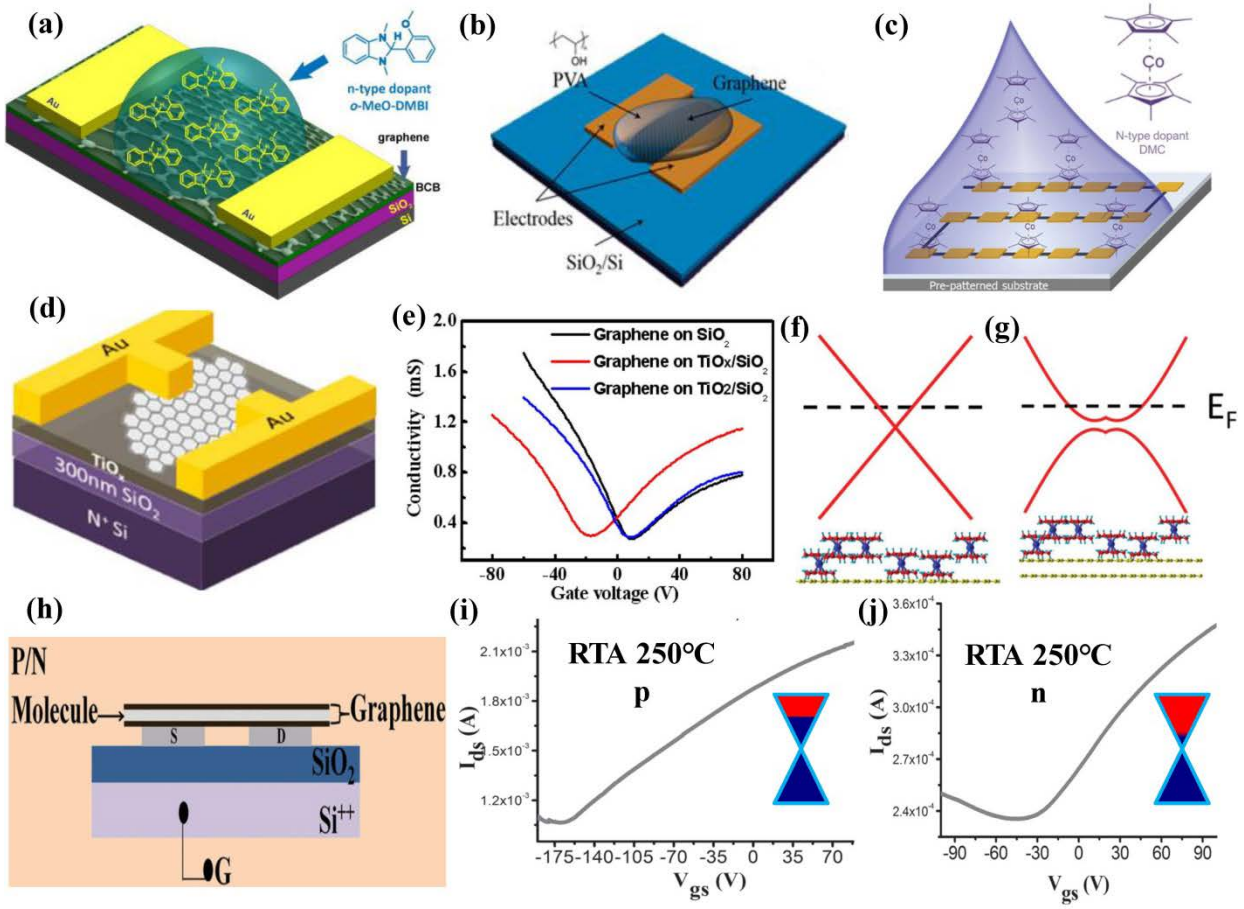

Figure 14 a) Schematic of FETs based on graphene doped with σ-MeO-DMBI. Reproduced with permission.[66] Copyright 2013, American Chemical Society. b) Schematic diagram of FETs based on polyvinyl alcohol (PVA) doped graphene. Reproduced with permission.[130] Copyright 2015, American Chemical Society. c) The representation of FETs array based on decamethylcobaltocene (DMC) doped graphene. Reproduced with permission.[131] Copyright 2015, Wiley-VCH. d) Schematic diagram of the TiOx self- encapsulation graphene device. e) Comparison of the electrical measurement results of a self-encapsulated graphene transistor. Reproduced with permission.[132] Copyright 2012, American Chemical Society. f-g) The bandgap of DMC-doped single- and double-layer mixed graphene ribbon. Reproduced with permission.[131] Copyright 2015, Wiley-VCH. h) Schematic diagram of FET based on graphene doped with P. i) and j) Electrical measurement results of FET based on P and N doped graphene, respectively.

Insets show schematic diagram of modulation of graphene Fermi level by doping. Reproduced with permission.[133] Copyright 2012, Wiley-VCH.

the adsorption of the ammonia molecules at the edge of graphene is relatively weak and could become unstable under high temperature leading to desorption. Therefore, there is a need to develop method that could yield stable n-type graphene. The adsorption doping of gaseousmolecules was first studied for p- type doping some time ago, before similar study was performed to develop n-type graphene. Such doping methods to change the conductivity type of graphene by gas molecules is known to result in unstable doped-graphene and its properties can be influenced by environmental factors, hence the study of the gas molecule-doped graphene would require expensive vacuum chamber and equipment *etc*. Such requirement for the study of the gas molecule-doped graphene and modulation of its conductive properties would raise questions on its research and application values due to its instability.

In addition to gas molecules-doped graphene, organic molecules and inorganic compounds adsorbed at the surface of graphene can also modulate its Fermi level above the Dirac point to form n-type graphene with electrons as majority carriers. Hayamizu[132] prepared n-type doped graphene sheet stripped mechanically by using a strong donor electron-organic material on graphene. The characterization results show that only TMPD-doped graphene exhibits n-type behavior among other organic materials (such as dibenzotetrathiafulvalene (DBTTF), 1,5-diaminonaphthalene (DAN) and hexamethyltetrathiafulvalene (HMTTF)). Even though these other organic materials are also considered as donor materials, they have lower energy levels than the work function of graphene (4.6 eV). This means that the choice of dopant also depend on its highest occupied state (HOMO), whereby the position of this state of the dopant must be higher than the work function of the graphene in order to form n-type graphene. FETs based on channel materials composed of graphene coated with σ-MeO-DMBI solution were fabricated and

characterized by Wei[66] and co-workers (as shown in the Figure 14a). The Dirac point of the graphene can be effectively regulated by the concentration of the solution, which changes graphene conductivity from p-type to n-type. In addition, Kim[130] *et al* prepared FETs based on channel material composed of graphene coated with polyvinyl alcohol (PVA) solution, which acts as a donor-doping agent, and annealed at different temperatures, as shown in Figure 14b. The study found that the Dirac point of its graphene coated with PVA at concentration of 20%wt is located at -40V after annealing at 150°C. Furthermore, the graphene exhibits stable n-type behavior even after exposure in air for days. Lee[131] and co-workers fabricated n-type graphene with single and double layer by using decamethylcobaltocene (DMC) (refer to Figure 14c). As characterized using Raman, the G and 2D peak of graphene shifted to higher wavenumber by 5 cm^{-1} and to lower wavenumber by 6 cm^{-1}, respectively at an increased concentration of DMC, which suggests n-type doping effect at the graphene. Ultraviolet photoelectron spectroscopy (UPS) was also performed to investigate the changes in the band structure of the single- and double-layer graphene after doping, as shown in Figure 14f and g. After doping, the Fermi energy level of single- and double-layer graphene is raised above the upper band of graphene due to the n-type doping effect. In addition to organic molecules, Chen[132] *et al* prepared self-encapsulated graphene with amorphous TiO_2, which is a typical donor material, as shown in Figure 14d. There is enormous difference in the doping effect when the graphene is encapsulated with TiO_2 as compared to TiO_x. FETs based on graphene encapsulated with TiO_x exhibit more obvious doping effect as compared to that with TiO_2. The Dirac point of TiO_x encapsulated graphene is located about -20 V while the Dirac point of graphene encapsulated with TiO_2 is essentially at the same position as those FETs with uncoated graphene, hence implying that the n-type graphene is mainly due to the presence of high density of oxygen vacancies in the TiO_x. Phosphorus-doped graphene is of interest in the development of n-type graphene. Lee[133] *et al* prepared and performed measurements on both phosphorus-doped and nitrogen-doped FETs as shown in Figure

14h. The Dirac points of the two graphene FETs are in negative bias, thus showing the effect of n-type doping. However, the Dirac points of the P-doped and N-doped graphene are located at approximately -170 V and -30 V, respectively after rapid thermal annealing (RTA) at 250°C, which indicates that the doping effect of the P-doped graphene is more significant than the N-

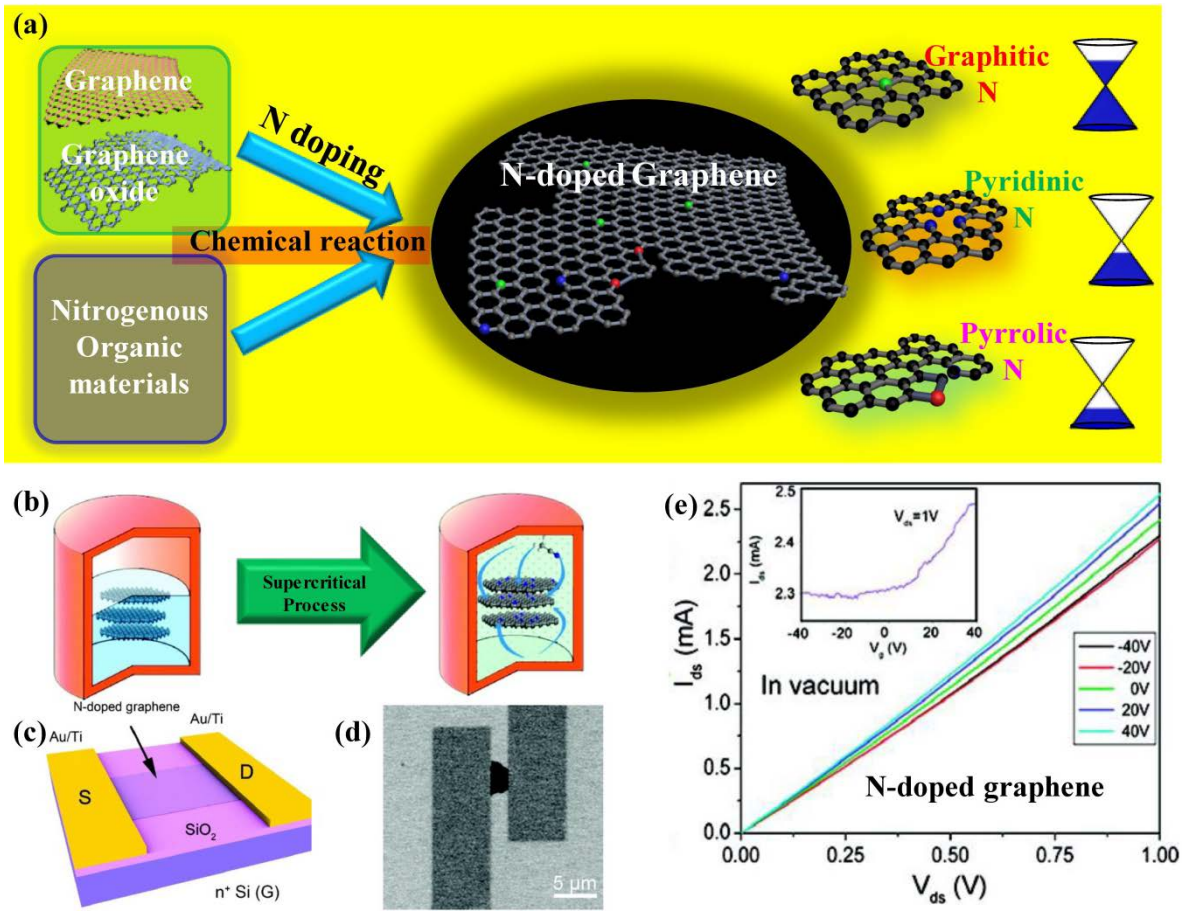

Figure 15 a) Schematic diagram of n-type graphene prepared by chemical methods. b) Preparation of nitrogen doped graphene by supercritical reaction. c) Schematic diagram of the FET based on few layer graphene doped with nitrogen via the supercritical method. d) SEM image of the FET based on nitrogen-doped few layer graphene prepared by supercritical reaction. e) The electrical measurement results of the FET based on nitrogen doped few layer graphene prepared by supercritical method. Reproduced with permission.[137] Copyright 2011, American Chemical Society.

doped, as shown in Figure 14i-j. Park[134] and co-workers transferred graphene onto the surface of phosphosilicate substrate and performed high temperature annealing to form stable n-type graphene. In addition, Lee[135] *et al* prepared n-type graphene by mixing ionic liquids with oxidized graphene and then performed annealing to reduce the graphene oxide. The doping effect is attributed to the ionic liquids, which can chemically modify the surface of graphene oxide. Fullerene derivatives are frequently used as donor electron materials in the field of optoelectronics, n-type graphene can be fabricated by doping with 0D fullerene on the 2D graphene, such study was performed by Jen[136] *et al*.

N-type graphene can also be prepared by doping with metals and its mechanism has been described in section 2.1.2. In general, electrons in the metal transfer to the graphene surface, forming n-type doping effect when graphene is in contact with metal, such as Al, Ag, and Cu, which has low work function. The adsorption doping of graphene by other substances are also reported, which mainly take advantage of transferring electrons of donor dopants to the surface of graphene, resulting in n-type doping effect. The advantage of these methods is that they do not lead to damage on the structure of graphene. However, the difficulty with n-type doping is that the exposed graphene is subjected to the adsorption of oxygen and vapor, which has p-type doping effect. The n-type doping requires the dopants to be able to transfer electrons to the surface of the graphene and compound the holes in graphene, resulting in graphene trans-type. Nonetheless, the stability of n-type graphene prepared by physical method still remains a major issue.

2.2.3 Chemical method to prepare n-type graphene

The chemical method to prepare n-type graphene has been fabricated either from intrinsic graphene, graphene oxide or organic polymers containing carbon and nitrogen atoms. The commonly used dopant to form n-type graphene is nitrogen atom, while the use of phosphorus atom has also been reported. As shown in Figure 15a, a nitrogen-doped graphene with n-type

conductivity is prepared by chemical reaction, which can result in three types of bonding between nitrogen and carbon atoms,[138] namely graphitic nitrogen, pyridinic nitrogen and pyrrolic nitrogen. The graphitic nitrogen can modulate the Fermi level of graphene to above the Dirac point, hence leading to n-type conductivity. However, both pyridinic and pyrrolic nitrogen does not produce n-type doping effect at the graphene. Schiros[139] *et al* performed DFT calculations on the work function of intrinsic and the three types of nitrogen bonding at graphene. The work function of intrinsic graphene is 4.43 eV, graphitic nitrogen is 3.98 eV, pyridinic nitrogen is 4.83 eV, and pyrrolic nitrogen is 4.92 eV. Based on the work function, it explains why the graphitic nitrogen can effectively modulate the Femi level of graphene to form n-type conductivity. Qian[137] *et al* prepared nitrogen-doped few-layer graphene with nitrogen content increases from 1.57 to 4.56 at % by chemical reaction on suspended graphite as the raw material at increasing reaction time from 2 to 24h in autoclave at 310 °C, as shown in Figure 15b. A FET was prepared by using the nitrogen-doped graphene as the channel material. The schematic diagram and SEM image of the FET are as shown in Figure 15c and d respectively. It can be seen that the prepared nitrogen-doped graphene films is of a few microns in size. The measurements of the FET are shown in Figure 15e, which shows the current density (I_{DS}) increases with increasing *Vg* from -40 V to +40 V. Furthermore, the Dirac point of the graphene is at the negative bias as shown in the inset, hence indicating n-type conductivity of the nitrogen-doped few-layer graphene prepared by the supercritical reaction.

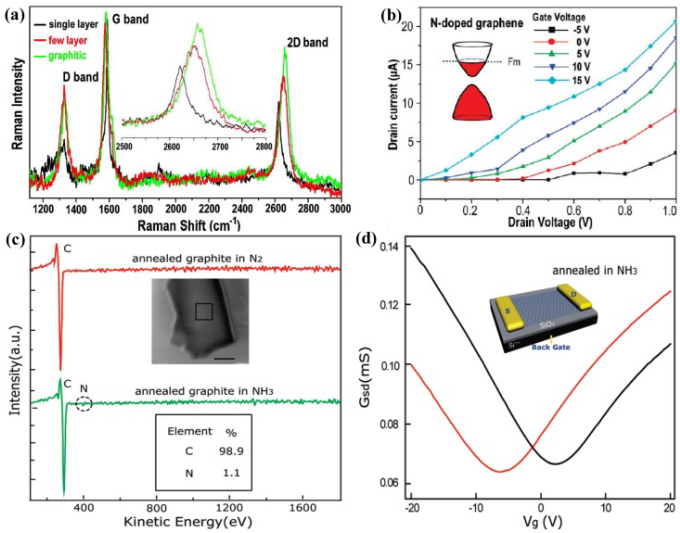

Figure 16 a) Raman spectra of nitrogen doped few layer graphene by chemical vapour deposition method. b) Electrical measurement results of FETs based on N-doped few layer graphene prepared by chemical vapor deposition method. Reproduced with permission.[140] Copyright 2009, American Chemical Society. c) Auger electron spectra of N-doped graphene prepared by irradiation with ammonia and nitrogen in the atmosphere. d) Electrical measurement results of FETs based on intrinsic graphene and n-doped graphene prepared by ammonia atmosphere irradiation. Reproduced with permission.[141] Copyright 2010, American Chemical Society.

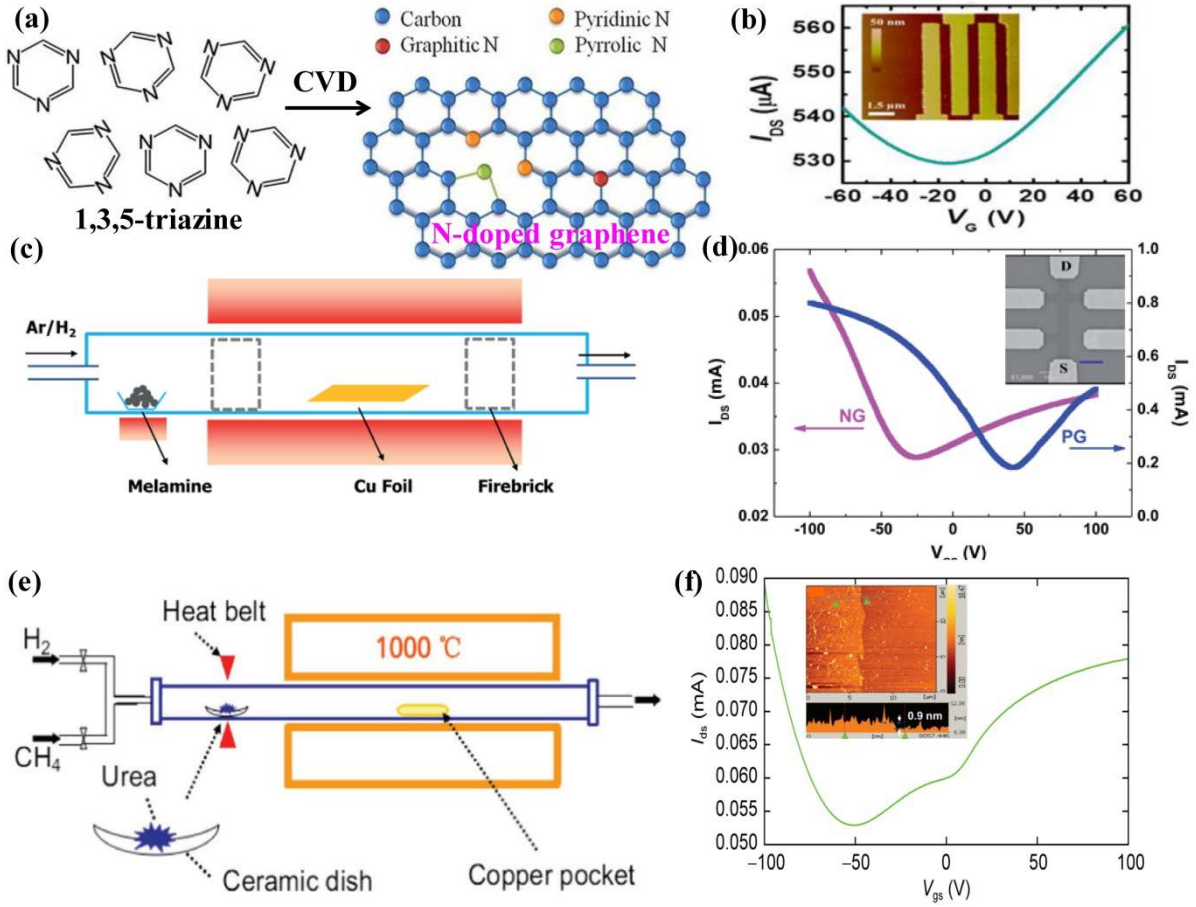

Figure 17 a) Schematic diagram showing nitrogen-doped graphene by 1,3,5-triazine. Reproduced with permission.[142] Copyright 2013, American Chemical Society. b) Electrical measurement results of FETs based on nitrogen-doped graphene prepared by graphite oxide, inset shows the AFM image of active channel regions. Reproduced with permission.[143] Copyright 2013, American Chemical Society. c-d) Schematic diagram of nitrogen-doped graphene prepared with melamine as carbon and nitrogen source, and its electrical measurement results, the inset of figure (d) shows the SEM image of FETs based on nitrogen-doped graphene prepared by this method. Reproduced with permission.[144] Copyright 2014, The Royal Society of Chemistry. e-f) Schematic of nitrogen doped graphene prepared with urea as carbon and nitrogen source, methane as auxiliary carbon source and the electrical measurement results of the transistors, the inset in figure (f) shows the AFM image of nitrogen-doped graphene obtained by this method and its thickness measurement. Reproduced with permission.[145] Copyright 2015, Springer.

In early 2009, Wei[140] and co-workers prepared nitrogen-doped graphene by CVD method in ammonia atmosphere that contributed to lattice doping of graphene. Raman characterization showed that the G peak of the single layer graphene prepared by the CVD method has down-shifted, which suggests n-type doping effect, as shown in Figure 16a. The nitrogen-doped graphene is then used to prepare a FET as channel material. Electrical measurements showed that the current density (I_{DS}) increases with increasing V_g from -5V to 15V, thus implying that the nitrogen-doped graphene prepared by the CVD method exhibits n-type conductivity as the Fermi level of the graphene is modulated above its Dirac point, as shown in Figure 16b. The calculated mobility is as high as 200 - 450 $cm^2V^{-1}s^{-1}$. In contrast, doping effect has not been observed by annealing graphene under N_2 atmosphere, which was demonstrated by Gong[141] *et al*. They prepared graphene by mechanical exfoliation method and annealed the graphene (which had undergone N^+-ion irradiation) in nitrogen and ammonia atmosphere. Studies performed on these post- annealed graphene using Auger electron spectroscopy, as shown in Figure 16c, reveal N elemental signal at graphene annealed in ammonia (equivalent to nitrogen content of 1.1%) but such signal is absent on graphene annealed in nitrogen. In order to further examine the doping of graphene by this method, a nitrogen-doped graphene FET was prepared and characterized as shown in Figure 16d. The Dirac point of the ammonia-annealed graphene is at a negative bias of about -8V, which indicates n-type conductivity, and the calculated charge mobility is up to 6000 $cm^2V^{-1}S^{-1}$.

Apart from the above-mentioned methods to prepare n-type graphene by doping intrinsic graphene, the preparation of N- doped graphene with nitrogen-containing organic polymers and oxidized graphene has been widely studied. Li[142] and co-workers fabricated N-doped graphene by utilizing 1, 3, 5-triazine as carbon and nitrogen source during CVD as illustrated in Figure 17a. The N-doped graphene was subsequently used as channel materials in FET and electrical measurements were performed on FETs with the doped graphene prepared at different

temperatures. The Dirac point of the graphene prepared at 700 and 800℃ is at negative bias implying that n-type graphene was successfully achieved. However, the highest charge mobility attained is 11.7 $cm^2V^{-1}s^{-1}$. Wang[144] *et al* fabricated nitrogen-doped graphene on a copper film by using high nitrogen melamine as carbon and nitrogen source as illustrated in Figure 17c. They prepared and performed electrical characterization on the nitrogen-doped graphene FET. It was found that the Dirac point was approximately at -25 V, which implies n-type conductivity at the graphene, as shown in Figure 17d. The calculated doping charge concentration is approximately 1.8×10^{12} cm^{-2}, and the charge mobility is 2 $cmV^{-1}s^{-1}$. The percentage of graphitic nitrogen in the total nitrogen content is about 40% as determined by XPS characterization. In addition, Wei[145] and co-workers prepared N-doped graphene by using urea as carbon and nitrogen source, and methane as a secondary carbon source using CVD method. Figure 17e illustrates the setup of the growth method. Atomic force microscopy measurement was performed on the as-grown film, which exhibits a thickness of 0.9 nm, hence indicating the film consists of a single layer of graphene as shown in inset of Figure 17f. A FET was fabricated using the graphene and electrical measurements were performed on the device. As can be seen from the measurement shown in Figure 2.16f, the Dirac point of graphene is located at -52.9 V. The calculated charge mobility is 74.1 $cm^2V^{-1}s^{-1}$ at nitrogen content of 3.72%. Graphene oxide can also produce n-type graphene via nitrogen-doping by treatment in a nitrogen-containing atmosphere. Huang[146] *et al* obtained a reduced graphene oxide with electron mobility of 29.08 $cm^2V^{-1}s^{-1}$ by annealing in NH_3. Baek[143] and co-workers prepared N-doped reduced graphene oxide by using graphene oxide to reduce nitrogen-containing small molecular polymers and fabricated a FET as shown in the inset of Figure 17b. From the electrical measurement results, shown in Figure 17b, the Dirac point of the graphene is located at -16 V implying that the graphene is of n-type conductivity. Also, the calculated electron mobility is 12.4 $cm^2V^{-1}s^{-1}$. Li[147] *et al* obtained N-doped graphene by using laser to reduce graphene oxide in the atmosphere of NH_3. The TEM image of reduced graphene

oxide thin films prepared by this method is shown at the top of Figure 18d and it can be seen that the film is very thin. Selective electron diffraction pattern (inset of Figure 18d) on the film reveals the crystal lattice of the graphene is of hexagonal structures. The thickness of the oxidized graphene on Si/SiO_2 substrate is characterized using cross-sectional SEM, as shown in the bottom image of Figure 18d, which indicates a film thickness of about 50 nm and reveals the homogeneity of the film. Figure 18c shows the electrical measurement performed on the FET using the doped graphene. The Dirac point of the graphene is at -8 V, which shows the characteristics of a n-type conductivity, and the calculated electron mobility is approximately 7.08 $cm^2V^{-1}s^{-1}$.

To date, most of the work on n-type graphene is based on nitrogen doping[148]. Co-doping of phosphorus and nitrogen from inorganic compound containing both nitrogen and phosphorus elements is also reported. Liu[149] and co-workers prepared P and N co-doped graphene films by using ethanol as carbon source, phosphonitrilic chloride trimer as phosphorus and nitrogen source in CVD method, as illustrated in Figure 18a. The content of nitrogen and phosphorus is reduced with increasing temperature from 700℃ to 1000℃, and the nitrogen atom is seen to reduce faster than the phosphorus atom. This suggests that the doping of phosphorus atoms is more stable. In order to show that the doping of the two atoms can modulate the electrical properties of graphene, FET based on the graphene doped with phosphorus and nitrogen was prepared, as shown in Figure 18b. Electrical measurement shows that the Dirac point is at negative bias of -40 V, implying that the co-doped graphene is of n-type conductivity. The calculated electron concentration is larger than 10×10^{12} cm^{-2} and the electron mobility is 8 - 12 $cm^2V^{-1}s^{-1}$. Previous work to prepare n-type graphene using chemical method has been focused mainly on nitrogen as dopants, and it is of interest to explore the use of other atoms as dopants. There are many reports on different chemical doping methods but the study on electrical properties of the doped graphene is still insufficient, especially on the mobility which require further attention.

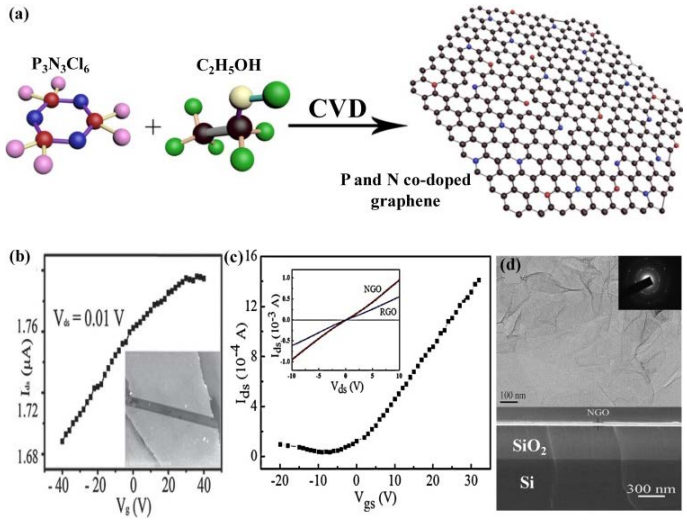

Figure 18 a) Schematic diagram of P and N co-doped graphene. b) Electrical measurement results of FETs based on P and N co-doped graphene, inset shows the SEM image. Reproduced with permission.[149] Copyright 2014, The Owner Societies. c-d) Characterization of the FET based on N-doped graphene oxide, TEM (top) and SEM cross-sectional images. Reproduced with permission.[147] Copyright 2015, AIP Publishing.

2.2.4 Other methods to prepare n-type graphene

Other methods to prepare n-type doped graphene have been described in section 2.1.4. Alternative method to prepare n-type graphene is very limited. Therefore, the preparation methods of n-type graphene are mainly in the forms of electrical, physical and chemical doping, as well as the localized doping method as previously described. More effort is needed to develop other effective doping methods. Next, we compare the relevant parameters of the p- and n-type graphene prepared by the various methods, as shown in Table 2. There is a clear rule when tabulating the parameters that is the physical doping method should not result in graphene lattice damage as it has detrimental effect on the properties of the graphene and limit its use in the p-n junction. While the chemical doping methods produce relatively stable doped-graphene, it could result in structural damage on the graphene by introducing defects and therefore resulting in declining performance of graphene, especially in carrier mobility. Although it is a preferential method for

the preparation of graphene p-n junction as the fabricated devices exhibit excellent electrical properties, there is a major issue in the reliability of the device performance. Its controllability on the carrier concentration is another critical issue to be addressed during the fabrication of p-n junction. Electrical doping method for the preparation of p- and n-type graphene does not have any major issue on the performance of graphene p-n junction, however there are significant challenges in applying the doping method on device structures. Therefore, future development on the doping methods for both p- and n-type graphene that has the ability to maintain the electrical properties of graphene and control its carrier concentration, which is suitable for device application, is of great scientific and commercial interests.

Table 2 Comparison of the different parameters of graphene with p- and n-type conductivity prepared by different preparation methods. (N/P/NG represent negtive/positive/not given)

Conductive type	Main-method	Sub-method	Doping source (work function)	Carrier mobility ($cm^2V^{-1}s^{-1}$)	Carrier concentration	Measured method	Measured temperature	Stability (N/P/NG)	Refs.
p type	Physical methods	Surface adsorption	F_4-TCNQ (5.24eV)	_	$3x10^{13}$ cm^{-2}	_	_	NG	[62]
		Surface adsorption	MoO_3 (6.8ev)	6150	$1.0x10^{13}$ cm^{-2}	FETs Calculated	300K	NG	[94]
		Surface adsorption	$NbCl_5$ (—)	85	$1.16x10^{19}$ cm^{-3}	Hall Test	300K	P	[97]
		Surface adsorption	$FeCl_3$ (5.2eV)	3650	$8.9x10^{14}$ cm^{-2}	Hall Test	_	P	[100]
	Chemical methods	CVD	Phenylboronic acid	800	_	FETs Calculated	300K	P	[105]
		CVD	Boric acid + Polystyrene	450-650	_	FETs Calculated	_	P	[107]
		CVD	Sulfur Powder + N-hexane	90	_	FETs Calculated	_	P	[111]
		CVD	H_2S+CH_4	68	_	FETs	_	N	[112]

						Calculated			
		Plasma treatment	Cl_2	1535	$1.2x10^{13}$ cm^{-2}	Hall Test	_	P	[115]
n type	Chemical methods	CVD	NH_3+CH_4	200-450	_	FETs Calculated	_	P	[140]
		Thermal annealing	NH_3	6000	_	FETs Calculated	_	N	[141]
		CVD	1,3,5-triazine	11.7	_	FETs Calculated	_	P	[142]
		Small molecule reduction method	GO+ Organic small molecule containing nitrogen	12.4	_	FETs Calculated	_	P	[143]
		CVD	Melamine	74	$1.8x10^{12}$ cm^{-2}	FETs Calculated	_	P	[144]
		CVD	Urea $+CH_4$	74.1	_	FETs Calculated	_	P	[145]
		Thermal annealing	NH_3+GO	29.08	_	FETs Calculated	_	N	[146]
		Laser reduction	NH_3+GO	7.08	_	FETs Calculated	_	N	[147]
		CVD	phosphonitrilic chloride trimer nitrile + Ethanol	8-15	$1x10^{12}$ cm^{-2}	FETs Calculated	_	P	[149]

3. Progress in the preparation of graphene homogeneous p-n junction

Although there are methods to prepare graphene with p- and n- type conductivity for the construction of p-n junction, there are key challenges to address in p-n junction, such as the interfacial states of p-type and n-type graphene. The graphene homogeneous p-n junction can be divided into three categories, namely electric field modulated graphene homogeneous p-n junction, in-plane graphene homogeneous p-n junction and vertical graphene homogeneous p-n junction.

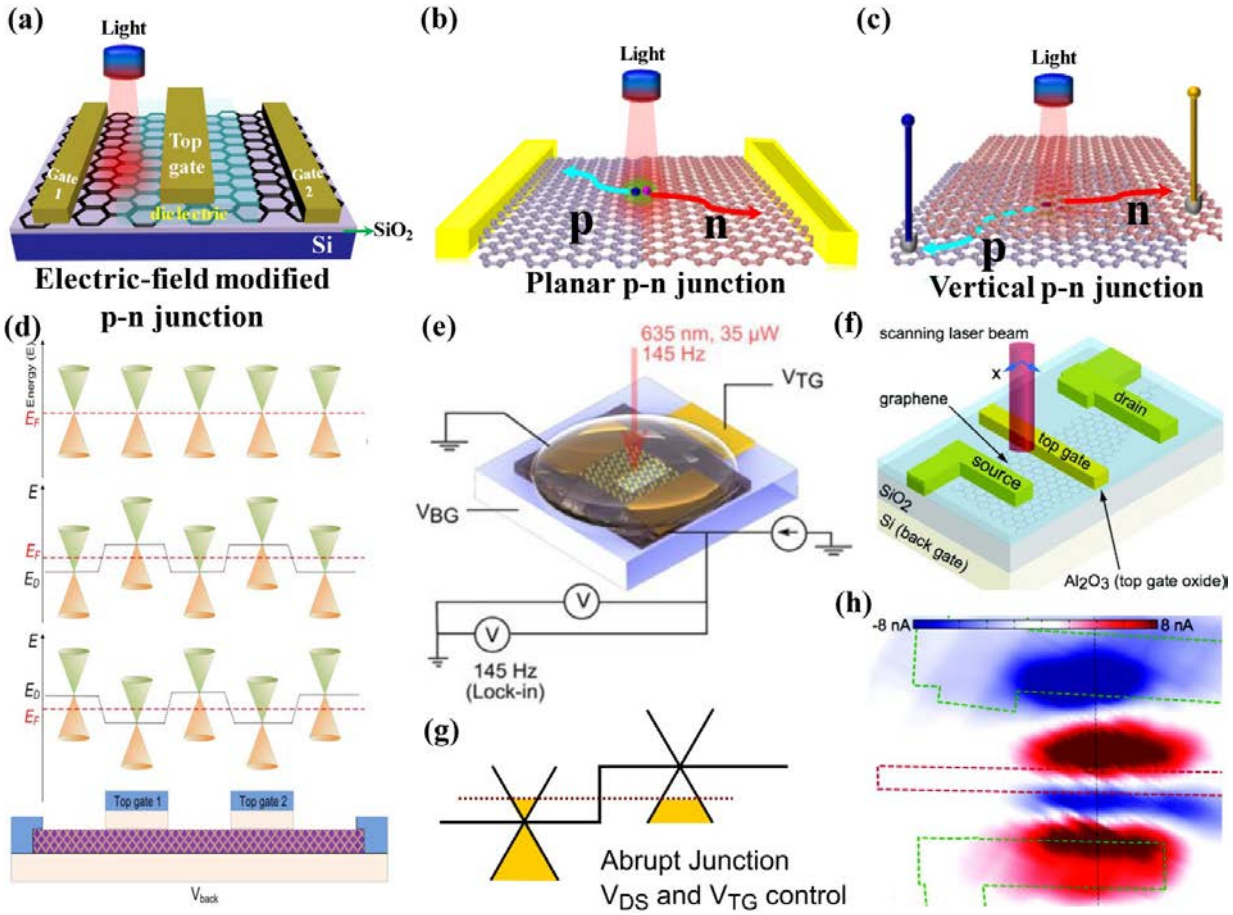

Figure 19 a-c) Schematic diagram showing the three different structures of graphene homogeneous p-n junction and mechanism of charge separation in photoelectron field. d) Schematic diagram of the band structure near the Dirac point in different areas of the device (as correlated to bottom diagram), band structure of V_{back} $=V_{tg1}=V_{tg2}=0$ V; V_{back} $=+0.2$ V, $V_{tg1}=V_{tg2}=-0.4$ V; V_{back} $=-0.4$ V, $V_{tg1}=V_{tg2}=+0.6$ V from top to bottom profiles, respectively. Reproduced with permission.[150] Copyright 2018, IOP Publishing. e) and g) Schematic diagram of device structure and energy band of the graphene p-n junction modulated by ion gate, respectively. Reproduced with permission.[151] Copyright 2017, Nature Publishing Group. f) and h) Schematic diagram of the photodetector consisting of electrically modulated graphene p-n junction and scanning optical current images of the device. Reproduced with permission.[152] Copyright 2011, American Chemical Society.

As shown in Figure 19a-c, the electric field modulated graphene homogeneous p-n junction relies on the use of electric field to provide local modulation of doping type at the graphene to form graphene homogeneous p-n junction, which has been explored for optoelectronics. The in-plane graphene homogeneous p-n junction is formed by p- and n-type graphene in the same plane. As photodetector, it is based on the FET structure, where electrons and holes are produced and separated in the same plane. The vertical graphene homogeneous p-n junction is referred to the stacking of differently doped-graphene in a vertical direction to form p-n junction. It is similar to traditional p-n junction, which electrons and holes are separated by an electric field in vertical direction, and the charge is transported in vertical direction for photodetector application. These three types of graphene homogeneous p-n junction have advantages and disadvantages in optoelectronics applications due to the different construction methods. Next, the application of photodetector based on the three different types of graphene homogeneous p-n junction will be discussed in detail.

3.1 Electric field modulated graphene homogeneous p-n junction

Electric field modulated graphene homogeneous p-n junction, which mainly uses the positive and negative bias at the gate terminate to modulate the Fermi level of the graphene, leading to a change in the conductive type of the local graphene hence directly constructing the graphene p-n junction. Nikiforidis[150] *et al* fabricated graphene homogeneous junctions consisting of n-p-n-p-n and p-n-p-n-p by using graphene as the channel material. A double top gate device is prepared and the Fermi energy level is modulated by applying voltages at both the top gates and back gate, as shown in Figure 19d. In addition to using metal electrode as the top gate, Grover[151] *et al* realized an abrupt p-n junction can be introduced at a double-layer graphene by using ionic liquids as the top gate material, as shown in Figure 19e. Besides, using ionic liquids as the top gate material had been carried out and investigated in earlier by Ye J. T.[153] et al. The energy

band structure of the graphene near the Dirac point can be constructed from the measured gate voltage plot, as shown in Figure 19g.

Further studies have found that the electrical properties and the photoelectric response of this p-n junction are related to the barrier height and temperature of the junction. For example, the PV effect of the junction increases with a decrease in temperature, which suggests that the thermal electrons are generated by the thermal excitation of the super crash. Marcus[152] and co-authors prepared top-gate photodetector based on graphene as shown in Figure 19f. By applying a voltage at the top and back gates, current image is obtained by the illumination of red light having a wavelength of 600 nm with a spot-size of approximately 0.5 μm as shown in Figure 19h. It can be seen from the figure that the light current is produced mainly near the top gate meaning the production of the current only occurs at the graphene p-n junction, hence demonstrating the important role of graphene p-n junction in the field of optoelectronics. The electric field moderated graphene homogeneous p-n junction is invaluable for the study of the electrical properties of graphene as well as applications in the field of optoelectronics. For example, Williams[154] *et al* prepared graphene p-n junction via using gate voltage, and studied the quantum Hall effect of graphene. In summary, a number of different electrically modulated graphene homogeneous p-n junctions have been reported.[155-157] There has been much research interests in its photoelectron applications[158,159] and energy band structure of graphene under gate voltage.[160,161] However, electrical modulation requires additional biases and specialized processes and equipment, which limit the practical application of such graphene homogeneous p-n junction.

3.2 In-plane graphene homogeneous p-n junction

In addition to the use of electrical field to develop p-n junction, doping graphene to form in-plane p-n junction is efficient and convenient as shown in Figure 20a. A depleted area with certain

width *L* can be introduced by diffusion of carriers between the p- and n-type graphene regions due to a difference in carrier concentration and type, as shown at the bottom of Figure 20a. There is diversity in the preparation methods used to fabricate the graphene homogeneous p-n junction, consisting of p- and n-type graphene front-end material. Shim[162] and co-workers fabricated locally doped n-type graphene by coating an organic polymers 6,13-bis (triisopropylsilylethynyl) pentacene (TIPS-pentacene) and applying laser irradiation, as shown in Figure 20b. As the graphene exhibits p-type in areas without laser irradiation, an in-plane p-n junction is formed and current can be observed under 532 nm laser irradiation, as shown in inset of Figure 20d. The maximum optical current of the graphene homogeneous p-n junction prepared using this method can reach 100 nA by modulating the Fermi levels of the graphene, as shown in Figure 20d. In addition, Yu[163] *et al* fabricated n-type graphene by performing electron beam irradiation on graphene at Si/SiO_2 substrate, which results in electrons transferring from the substrate to the graphene hence forming n-type graphene. Graphene is converted from p- to n-type through local irradiation. A light sensitive photoelectric transistor based on FET with graphene p-n junction as channel material prepared via electron beam was fabricated as shown in Figure 20c. Under 532

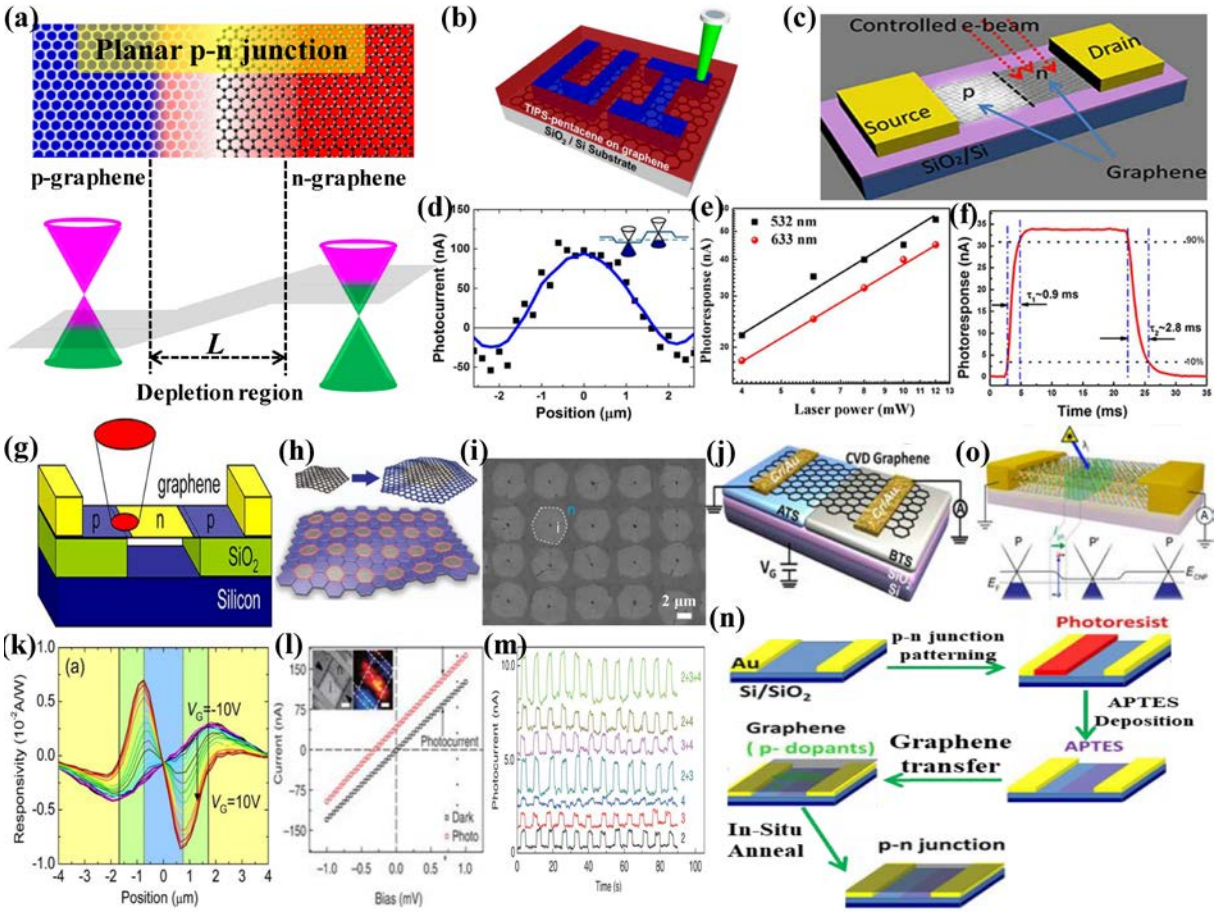

Figure 20 a) Schematic diagram showing in-plane graphene homogeneous p-n junction (top diagram), the band structure of in-plane graphene homogeneous p-n junction (bottom diagram). b) Schematic diagram on the preparation of in-plane graphene homogeneous p-n junction by direct laser writing. Reproduced with permission.[162] Copyright 2014, American Chemical Society. c) Schematic on the preparation of graphene homogeneous p-n junction by controllable electron beam irradiation. Reproduced with permission.[163] Copyright 2015, Nature Publishing Group. d) The plot of photoelectric responsivity and position for graphene homogeneous p-n junction prepared by laser direct writing. Reproduced with permission.[162] Copyright 2014, American Chemical Society. e) and f) display plots of current and irradiation power for photodetectors based on graphene homogeneous p-n junction prepared by electron beam irradiation under 532 nm and the 633 nm irradiation and its response time under 633 nm irradiation. Reproduced with permission.[163] Copyright 2015, Nature Publishing Group. g) Schematic diagram of photodetector

based on suspended graphene. Reproduced with permission.[164] Copyright 2013, American Chemical Society. h) Schematic diagrams of the modulated-doped growth (top diagram) and inlaid graphene (bottom diagram), which the different coloured areas represent different doped graphene. i) SEM image of inlaid-type graphene at random regions. Reproduced with permission.[165] Copyright 2012, Nature Publishing Group. j) Representation of in-plane graphene p-n junction on Si/SiO2 substrate modified by N-butyltriethoxysilane (BTS) and 3-aminopropyltriethoxysilane (ATS). Reproduced with permission.[166] Copyright 2015, IOP Publishing. k) Plot of responsivity-position at different gate voltage. Reproduced with permission.[164] Copyright 2013, American Chemical Society. l) and m) display plots of current and bias of graphene homogeneous p-n junction under 633 nm laser irradiation and response time graphs of each channel respectively. Reproduced with permission.[165] Copyright 2012, Nature Publishing Group. n) Schematic diagrams showing the preparation process of in-plane graphene homogeneous p-n junction. Reproduced with permission.[167] Copyright 2012, American Chemical Society. o) Diagram of structure (top) and bandgap (bottom) of homojunctions of $FeCl_3$ doped graphene. Reproduced with permission.[168] Copyright 2017, Wiley-VCH.

nm and 633 nm illumination, the output current of the graphene homogeneous p-n junction increases as the power of the light increases, as shown in Figure 20e. From Figure 20f, it can be seen that the photoelectric response time of such homogeneous p-n junction can reach millisecond scale under 633 nm illumination with rise time of 0.9 ms and fall time of 2.8 ms. The detectivity of such photoelectric detector is approximately 3.0×10^{10} $cmHz^{1/2}$ W^{-1} at room temperature, which is comparable to the photoelectric detectors based on III-V family.

Besides applying electron beam and laser irradiation, graphene homogeneous p-n junction can also be formed by suspending graphene over a substrate as demonstrated by Freitag[164] and co-workers (refer to Figure 20g). They identified graphene homogeneous p-n junction in area

between graphene with substrate support and in suspension as studied using light current characterization, which found larger current density at suspended graphene than on supported structures. Analysis of the responsivity curve and position of such photodetector suggested that the detector is based on photothermal mechanism. Under 476 nm illumination, the responsivity at room temperature is approximately $1x10^{-2}$ AW^{-1}, as shown in Figure 20k. Liu[165] *et al* performed nucleation and epitaxial growth of graphene using methane and acetonitrile in CVD method respectively. Figure 20h illustrates the growth mechanism. SEM image of the embedded graphene is displayed in Figure 20i. Acetonitrile, which contains nitrogen, is used to prepare the n-type graphene, while the methane is used to produce the intrinsic graphene. The inlaid graphene structures produce numerous nanometer graphene p-n junctions on the entire surface through the replacement growth process. Photoelectric measurements were performed under 633 nm irradiation and the results are shown in Figure 20l. It can be seen that the optical current increases significantly during illumination and the current generation is mainly at the p-n junction, which again explains the importance of constructing graphene p-n junction for the field of optoelectronics. Measurement of the photoelectric response time of such junction exhibits a fasterresponse time than the individual channel as shown in Figure 20f. In addition, Wang[166] and co-workers prepared p- and n-type doped graphene by utilizing a differently treated substrates, as shown in Figure 20j. Two local ATS and BTS materials are coated on a Si/SiO_2 substrate prepared via electron beam lithography and graphene is then transferred onto the substrate to form n- and p-type doping zone. The FET based on this in-plane graphene homogeneous p-n junction also shows photoelectric response under the irradiation of 532 nm visible light. Its external quantum effect (*EQE*) is approximately 0.15%, which attributes to the visible absorption of graphene of about 2.3% and at a junction area of only 200 nm. Similar method to prepare such structure was also performed by Baltazar[167] and the preparation process is illustrated in Figure 20n. The recently discovered laser written homojunctions of $FeCl_3$ doped graphene which exhibit

an extraordinary linear dynamic range in their photoresponse, as shown in Figure 20o. This important work had been carried out by Sanctis Adolfo De[168] et al, this functionalized graphene photodetector exhibited extraordinary linear response and linear dynamic range (LDR) value lager than that of other graphene devices at least 4500 time (44 dB). Much work is still needed in the development of a practical, facile preparation method that can produce graphene homogeneous p-n junction. The methodology can utilize the unique physical and chemical properties of the graphene materials. Preparation of large size and high quality in-plane graphene p-n junction remains a challenge. However, there is some progress made in the understanding of the physical properties of graphene homogeneous p-n junction.[169-171] Furthermore, a variety of preparation methods[162-167,172] are also in the developmental phase.

3.3 Vertical graphene homogeneous p-n junction

Apart from electric field modulated and in-plane graphene homogeneous p-n junctions, vertical graphene homogeneous p-n junction is also of great interests and has been constructed similar to the traditional p-n junction. Due to the physical properties of the graphene, the vertical graphene homogeneous p-n junction is formed by the van der Waals force between p- and n-type graphene

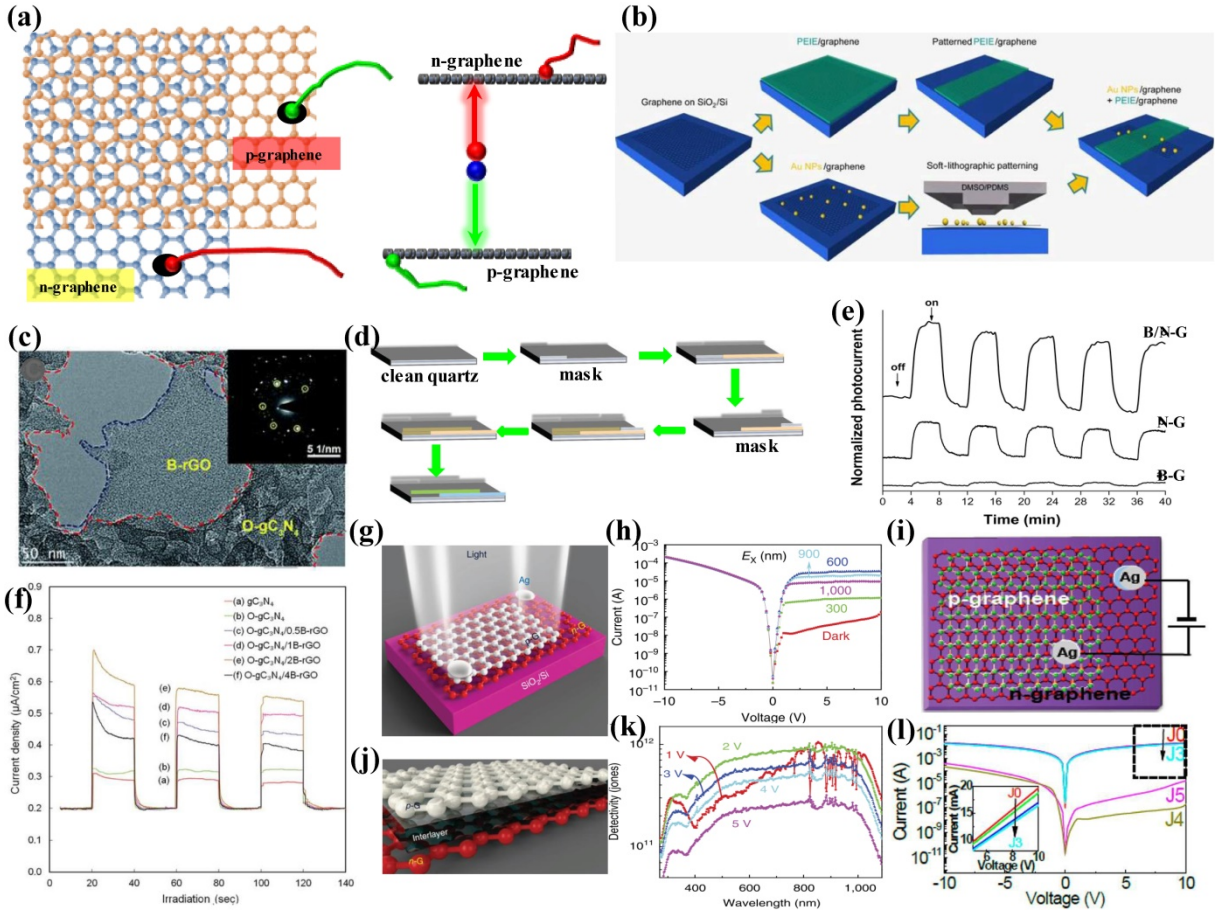

Figure 21 a) Schematic diagrams showing the structure of vertical graphene homogeneous p-n junction, top view (left) and side view (right). b) Schematic of the preparation process of vertical graphene homogeneous p-n junction prepared by plate printing. Reproduced with permission.[173] Copyright 2015, Wiley-VCH. c) TEM image of vertical graphene homogeneous p-n junction, inset shows the selection of electron diffraction (SAD) image. Reproduced with permission.[174] Copyright 2018, The Royal Society of Chemistry. d) and e) Schematic diagram illustrating the preparation process of the vertical graphene homogeneous p-n junction composed of B-G/N-G graphene and the response time plots of the three different optoelectronic devices respectively. Reproduced with permission.[175] Copyright 2014, Wiley-VCH. f) Transient response time plots of different graphene optoelectronic devices. Reproduced with permission.[174] Copyright 2018, The Royal Society of Chemistry. g-h) and j-k) Schematic diagrams of photodetector based on vertical graphene homogeneous p-n junction and its performance respectively. Reproduced with permission.[176] Copyright 2014, Nature Publishing Group. i) and l) Schematic diagram of vertical

graphene homogeneous p-n junction and its I-V measurement results respectively. Reproduced with permission.[177] Copyright 2013, American Chemical Society.

layers. As shown in Figure 21a, the vertical graphene homogeneous p-n junction, whose p- and n-type graphene layers are stacked vertically and the charge transport is mainly in the vertical direction. As graphene has a thickness of a single atom, the charge transport in the vertical direction is therefore more rapid and effective. This explains why the vertical graphene homogeneous p-n junction exhibits much better performances than the in-plane ones. However, the vertical graphene homogeneous p-n junction is still very rare because of the technical difficulty in its construction. An[173] *et al* prepared n- and p-type graphene by using ethoxylated polyethylenimine (PEIE) and gold nanoparticles, respectively. Flat-panel printing technology is then used to produce a vertically stacked graphene homogeneous p-n junction. Figure 21b illustrates the preparation process. Such preparation method has successfully produced transparent and flexible graphene nano-devices exhibiting excellent performances. Another interesting method[177] was reported that utilize reduced graphene oxide (rGO) and boric acid to prepare B-doped graphene. During the synthesis process, oxygen-doped C_3N_4 (O-gC_3N_4) was then added to the B-doped graphene solution, which resulted in O-gC_3N_4/B-rGO hybrid nanocomposite. Figure 21c shows the TEM image that reveals the formation of the O-gC_3N_4/B-rGO hybrid nanocomposite. Besides, the O-gC_3N_4/B-rGO forms a stack compound, which O-gC_3N_4 and B-rGO exhibit n- and p-type conductivity respectively, thus forming a vertical graphene homogeneous p-n junction. Photoelectric measurement was performed on this p-n junction, which exhibits exceptional response to light with maximum optical current intensity as shown in the transient analysis in Figure 21f. The use of electron beam lithography to produce a vertically structured graphene homogeneous p-n junction was performed by García[175] and co-workers, as illustrated in Figure 21d. N-type graphene doped with N (N-G) was produced by pyrolysis of

chitosan film at 900°C, while p-type graphene doped with B (B- G) was produced by pyrolysis of alginate, and their corresponding electrical performance was obtained by Hall measurements. Vertically stacked graphene homogeneous p-n junction was then constructed using electron beam lithography. Figure 21e shows the measurements of three different photoelectric transient responses. It can be seen that the graphene homogeneous p-n junction consisting of the B-G/N-G has the largest photocurrent, hence implying that the graphene p-n junction exhibits better photoelectric performance than other devices that do not comprise of p-n junction. Therefore, the graphene p-n junction has an important role in the applications of optoelectronics. To improve the performance of the vertical graphene homogeneous p-n junction, Kim[176] *et al* fabricated the vertical p-n junction consisting of p-type graphene doped with $AuCl_3$ laying on top of n-type graphene doped with 1,10-dibenzyl-4,40-bipyridinium with an interlayer between the two differently doped graphene, which results in a reduction on the dark current of the graphene p-n junction. Figure 21g and j show the top and side views of the fabricated device structure respectively. Photodetectors prepared using this method exhibit a detectivity of up to 10^{12} $cmHz^{-1/2}W^{-1}$ and a response band is observed between 300 nm to 1000 nm as shown in Figure 21h and k respectively. The interlayer between the p- and n-type graphene can effectively restrain the dark current of the graphene photodetector hence resulting in an improved performance. Moreover, a stable performance of up to six months is observed on the photodetector. Kim[177] and co-authors performed further study on such vertical graphene homogeneous p-n junction as shown in Figure 21i. I-V measurements, shown in Figure 21l, reveals on-off ratio of 10^3. This demonstrates the effectiveness of the methodology in preparing the photodetector based on the vertical graphene homogeneous p-n junction. The vertical structure of the p-n junction utilizes the advantages of vertical charge transport, similar to the traditional p-n junction, and the unique properties of graphene materials to produce high-performance devices that are suitable for applications in the optoelectronics field.

Finally, the performance of photodetectors based on the three main types of graphene homogeneous p-n junction is summarized in Table 3. As can be seen from the Table, most studies were performed using FET device structure consisting of graphene homogeneous p-n junction. It is worth noting that the photodetector based on the vertical structure of the graphene homogeneous p-n junction exhibits the best performance as compared to those based on the electric field modulation and the in-plane structure, hence indicating the future direction of device structure consisting of graphene homogeneous p-n junction.

4. Perspectives and overviews of graphene homogeneous p-n junction

This paper provides a comprehensive review on the preparation of p- and n-type graphene, and its construction of homogeneous p-n junction based on different methodologies and structures. The requirements on developing high-performance front-end materials for photodetector as well as the

Table 3 The performance of photodetector based on different structures of graphene homogeneous p-n junction.

Structure of graphene homogeneous p-n junction	Device structure	Response wavelength (nm)	Response time	Responsivity	Detectivity ($cmHz^{-1/2}W^{-1}$)	*EQE*	LDR (dB)	Refs.
Electrical modulation	FETs- Ion gate	635	_	600 mVW^{-1}	_	_	_	[151]
	FETs- Metal gate	532	_	1.5x10^{-3} AW^{-1}	_	_	_	[152]
	FETs- Metal gate	514.5	_	3x10^{-4} AW^{-1}	_	_	_	[158]
Planar structure	FETs	532	_	~1x10^{-4} AW^{-1}	_	_	_	[162]
	FETs	633	0.9 ms	_	~3x10^{10}	_	_	[163]
	FETs	476	_	2.7x10^{-3} AW^{-1}	_	_	_	[164]
	FETs	633	_	1x10^{-4} AW^{-1}	_	_	_	[165]
	FETs	532	_	_	_	0.15%	_	[166]
	FETs	375-10000	_	0.1 mA W^{-1}	_	_	44	[168]
Vertical structure	_	300-1000	40 μ s	0.4-1.0 AW^{-1}	~10^{12}	_	93	[176]

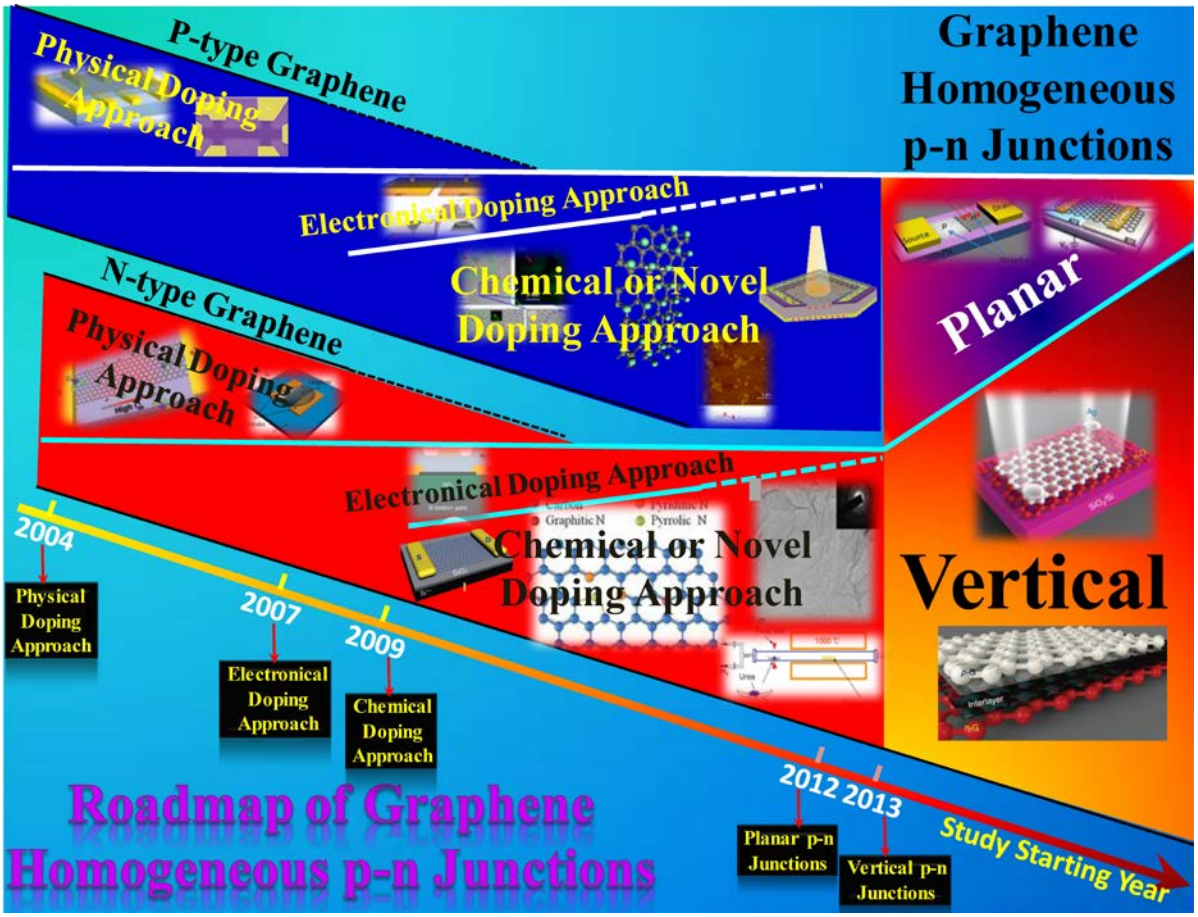

Figure 22 Development roadmap of graphene homogenous p-n junctions including different preparation methods to fabricate p or n-type graphene.

merits and drawbacks of the different p-n junction structures have been discussed. The suitability of the preparation technique to construct the graphene homogeneous p-n junction will depend on the requirements and applications of the devices. As for drawbacks and merits of different preparations and junctions, the roadmap of graphene homogenous p-n junction is displayed in Figure 22. However, the development of those approaches and junctions can be clearly foreseen that chemical or novel method to fabricate p or n-type graphene will become mainstream due to

stability and realism and so on. According to current research about graphene p-n junctions, the various parameters of vertical junction commonly higher than that of planar junction due to high efficiency of carriers separation and short transport distance and so on. This review has discussed some challenges on the preparation of graphene with p- and n-type conductivity and its construction of the p-n junction. Some thoughts on the future development of graphene p-n junction for the optoelectronics industry have also been put forward. Above all, this paper provides some ideas on enhancing the performance of optoelectronic devices based on graphene p-n junction.

Acknowledgements

This work was supported by National Natural Science Foundation of China (Grant Nos. 61106098, 51201150, 11374250 and 11864044), the Key Project of Applied Basic Research of Yunnan Province, China (Grant No. 2012FA003), PolyU grants (1-ZVGH and 1-BBAD) and Research Grants Council of Hong Kong (Project nos: PolyU 153030/15P, PolyU 153271/16P and PolyU 153039/17P).

Received: ((will be filled in by the editorial staff))

Revised: ((will be filled in by the editorial staff))

Published online: ((will be filled in by the editorial staff))

References

[1] Z.-X. Zhang, D. Li, *Acta Phys. Sin.* **2017**, *21*, 217302.

[2] T. Li, J. R. Hauptmann, Z. Wei, S. Petersen, N. Bovet, T. Vosch, J. Nygård, W. Hu, Y. Liu, T. Bjørnholm, K. Nørgaard, B. W. Laursen, *Adv. Mater.* **2012**, *24*, 1333.

[3] H. T. Das, K. Mahendraprabhu, T. Maiyalagan, P. Elumalai, *Sci. Rep.* **2017**, *7*, 15342.

[4] L.-Q. Tao, Y. Liu, H. Tian, Z.-Y. Ju, Q.-Y. Xie, Y. Yang, T.-L. Ren, *AIP Advances* **2016**, *6*, 015105.

[5] H. Sun , X. You , J. Deng , X. Chen , Z. Yang , J. Ren , H. Peng, *Adv. Mater.* **2014**, *26*, 2868.

[6] X. Yin, C. S. Tang, D. Wu, W. Kong, C. Li, Q. Wang, L. Cao, M. Yang, Y.-H. Chang, D. Qi, F. Ouyang, S. J. Pennycook, Y. P. Feng, M. B. H. Breese, S. J. Wang, W. Zhang, A. Rusydi, A. T. S. Wee, *Adv. Sci.* **2019**, 1802093.

[7] A. Rampello, P. Papi, G. Pompa, A. Rampello, A. Polimeni, C. Di Paolo, *Eur. Rev. Med. Pharmacol. Sci.* **2018**, *22*, 1180.

[8] L. Zhang, Z. Yu, L. Zhang, X. Zheng, L. Xiao, S. Jia, J. Wang, *J. Mater. Chem. C* **2018**, *6*, 2460.

[9] M. C. Robbins, S. J. Koester, *IEEE Electron Device Letters* **2017**, *38*, 285.

[10] M. Chen, *Proceedings of the IEEE* **2005**, *93*, 1339.

[11] K. Jagiela, *Electric Machines & Power Systems* 1**985**, *10*, 15.

[12] I. Amit, T. J. Octon, N. J. Townsend, F. Reale, C. D. Wright, C. Mattevi, M. F. Craciun, S. Russo, *Adv. Mater.* **2017**, *29*, 1605598.

[13] M. A. Loi, C. Rost-Bietsch, M. Murgia, S. Karg, W. Riess, M. Muccini, *Adv. Funct. Mater.* **2006**, *16*, 41.

[14] D. Jariwala, V. K. Sangwan, D. J. Late, J. E. Johns, V. P. Dravid, T. J. Marks, L. J. Lauhon, M. C. Hersam, *Appl. Phys. Lett.* **2013**, *102*, 173107.

[15] J. G. Lee, S. Masui, *IEICE Electronics Express* **2012**, *9*, 477.

[16] P. F. Siles, B. S. Archanjo, D. L. Baptista, V. L. Pimentel, J. Joshua, B. R. A. Neves, G. M. Ribeiro, *J. Appl. Phys.* **2011**, *110*, 024511.

[17] M. Kang, K.-W. Song, B.-G. Park, H. Shin, *Microelectronics Journal* **2011**, *42*, 837.

[18] Zs.J. Horváth, *Current Applied Physics* **2006**, *6*, 145.

[19] G. Agnus, A. Filoramo, S. Lenfant, D. Vuillaume, J.-P. Bourgoin, V. Derycke, *Small* **2010**, *6*, 2659.

[20] S. Abdellatif, K. Kirah, *Opt. Lett.* **2013**, *38*, 3680.

[21] M. Freitag, Y. Martin, J. A. Misewich, R. Martel, Ph. Avouris, *Nano Lett.* **2003**, *3*, 1067.

[22] E. Knill, R. Laflamme, G. J. Milburn, *Nature* **2001**, *409*, 4.

[23] H. Li, Z. Yin, Q. He, H. Li, X. Huang, G. Lu, D. W. H. Fam, A. I. Y. Tok, Q. Zhang, H. Zhang, *Small* **2012**, *8*, 63.

[24] T. Kuila, S. Bose, P. Khanra, A. K. Mishra, N. H. Kim, J. H. Lee, *Biosensors and Bioelectronics* **2011**, *26*, 4637.

[25] P. Solis-Fernandez, M. Bissett, H. Ago, *Chem. Soc. Rev.* **2017**, *46*, 4572.

[26] W. Zhang, L. Wu, Z. Li, Y. Liu, *Rsc Adv* **2015**, *5*, 49521.

[27] Y.-W. Son, M. L. Cohen, S. G. Louie, *Nature* **2006**, *444*, 347.

[28] C. Lee, X. Wei, J.W. Kysar, J. Hone, *Science* **2008**, *321*, 385.

[29] R.R. Nair, P. Blake, A.N. Grigorenko, K.S. Novoselov, T.J. Booth, T. Stauber, N.M.R. Peres, A.K. Geim, *Science* **2008**, *320*, 1308.

[30] K.I. Bolotin, K.J. Sikes, Z. Jiang, M. Klima, G. Fudenberg, J. Hone, P. Kim, H.L. Stormer, *Solid State Commun.* **2008**, *146*, 351.

[31] A.A. Balandin, S. Ghosh, W. Bao, I. Calizo, D. Teweldebrhan, F. Miao, C.N. Lau, *Nano Lett.* **2008**, *8*, 902.

[32] M.F. Craciun, S. Russo, M. Yamamoto, S. Tarucha, *Nano Today* **2011**, *6*, 42.

[33] W.J. Yu, L. Liao, S.H. Chae, Y.H. Lee, X. Duan, *Nano Lett.* **2011**, *11*, 4759.

[34] X. Fan, Z. Shen, A.Q. Liu, J. Kuo, *Nanoscale* **2012**, *4*, 2157.

[35] T. Hu and I.C. Gerber, *Chem. Phys. Lett.*, **2014**, *616-617*, 75.

[36] Y. Guo, W. Guo, C. Chen, *Appl. Phys. Lett.* **2008**, *92*, 243101.

[37] P. Shemella, S.K. Nayak, *Appl. Phys. Lett.* **2009**, *94*, 32101.

[38] M. Y. Han, B. Özyilmaz, Y. Zhang, P. Kim, *Phys. Rev. Lett.* **2007**, *98*, 206805.

[39] A.K. Singh, E.S. Penev, B.I. Yakobson, *ACS Nano* **2010**, *4*, 3510.

[40] T. Ohta, A. Bostwick, T. Seyller, K. Horn, E. Rotenberg, *Science*, **2006**, *313*, 951.

[41] T. Khodkov, I. Khrapach, M. F. Craciun, S. Russo, *Nano Lett.* **2015**, *15*, 4429.

[42] Y. Zhang, T. Tang, C. Girit, Z. Hao, M.C. Martin, A. Zettl, M.F. Crommie, Y.R. Shen, F. Wang, *Nature* **2009**, *459*, 820.

[43] D.C. Elias, R.R. Nair, T.M.G. Mohiuddin, S.V. Morozov, P. Blake, M.P. Halsall, A.C. Ferrari, D.W. Boukhvalov, M.I. Katsnelson, A.K. Geim, K.S. Novoselov**, *Science*** 2009, ***323***, **610**.

[44] X. Fan, L. Liu, J. Kuo, Z. Shen, *The Journal of Physical Chemistry C* **2010**, *114*, 14939.

[45] T.O. Wehling, K.S. Novoselov, S.V. Morozov, E.E. Vdovin, M.I. Katsnelson, A.K. Geim, A.I. Lichtenstein, *Nano Lett.* **2008**, *8*, 173.

[46] S.Y. Zhou, G.H. Gweon, A.V. Fedorov, P.N. First, W.A. de Heer, D.H. Lee, F. Guinea, A.H. Castro Neto, A. Lanzara, *Nat. Mater.* **2007**, *6*, 770.

[47] E. Rotenberg, A. Bostwick, T. Ohta, J.L. McChesney, T. Seyller, K. Horn, *Nat. Mater.* **2008**, *7*, 258.

[48] F. Schwierz, *Nat. Nanotechnol.* **2010**, *5*, 487.

[49] T.S. Li, S.C. Chang, Y.C. Chuang, K.H.J. Wu, M.F. Lin, *Physica B: Condensed Matter* **2009**, *404*,

305.

[50] Z. Yan, Z. Sun, W. Lu, J. Yao, Y. Zhu, J.M. Tour, *ACS Nano* **2011**, *5*, 1535.

[51] S. Bala Kumar, T. Fujita, G. Liang, *J. Appl. Phys.* **2011**, *109*, 73704.

[52] S.J. Goncher, L. Zhao, A.N. Pasupathy, G.W. Flynn, *Nano Lett.* **2013**, *13*, 1386.

[53] S. Nakaharai, T. Iijima, S. Ogawa, S. Suzuki, S. Li, K. Tsukagoshi, S. Sato, N. Yokoyama, *ACS Nano* **2013**, *7*, 5694.

[54] X. Zheng, M. Feng, Z. Li, Y. Song, H. Zhan, *J. Mater. Chem. C* **2014**, *2*, 4121.

[55] Y. Zhu, J. Lian, Q. Jiang, *Chem. Phys. Chem.* **2014**, *15*, 958.

[56] Z. Lin, W. Qin, J. Zeng, W. Chen, P. Cui, J. Cho, Z. Qiao, Z. Zhang, *Nano Lett.* **2017**, *17*, 4013.

[57] G. Seol, J. Guo, *Appl. Phys. Lett.* **2011**, *98*, 143107.

[58] S. Kamikawa, T. Shimizu, Y. Yagi, J. Haruyama, *Nanomater. Nanotechno.* **2014**, *4*, 12.

[59] L. Lin, L. Liao, J. Yin, H. Peng, Z. Liu, *Nano Today* **2015**, *10*, 701.

[60] P. K. Herring, A. L. Hsu, N. M. Gabor, Y. C. Shin, J. Kong, T. Palacios, P. Jarillo-Herrero, *Nano Lett.* **2014**, *14*, 901.

[61] E. Rossi, J. H. Bardarson, P. W. Brouwer, *ECS Transactions* **2011**, *35*, 271.

[62] H. Oh, S. Coh, Y.-W. Son, M. L. Cohen, *Phys. Rev. Lett.* **2016**, *117*, 016804.

[63] V. V. Cheianov, V. Fal'ko, B. L. Altshuler, *Science* **2007**, *315*, 1252.

[64] H. Chiu, V. Perebeinos, Y. Lin, P. Avouris, *Nano Lett.* **2010**, *10*, 4634.

[65] F. Schedin, A.K. Geim, S.V. Morozov, E.W. Hill, P. Blake, M.I. Katsnelson, K.S. Novoselov, *Nat. Mater.* **2007**, *6*, 652.

[66] P. Wei, N. Liu, H.R. Lee, E. Adijanto, L. Ci, B.D. Naab, J.Q. Zhong, J. Park, W. Chen, Y. Cui, Z.

Bao, *Nano Lett.* **2013**, *13*, 1890.

[67] F. Yavari, C. Kritzinger, C. Gaire, L. Song, H. Gulapalli, T. Borca-Tasciuc, P.M. Ajayan, N. Koratkar, *Small*, **2010**, *6*, 2535.

[68] M.D. Stoller, S. Park, Y. Zhu, J. An, R.S. Ruoff, *Nano Lett.* **2008**, *8*, 3498.

[69] E. T. Alonso, D. P. Rodrigues, M. Khetani, D.-W. Shin, A. De Sanctis, H. Joulie, I. de Schrijver, A. Baldycheva, H. Alves, A. I. S. Neves, S. Russo, M. F. Craciun, *npj Flexible Electronics* **2018**, *2*, 25.

[70] K.F. Mak, C.H. Lui, J. Shan, T.F. Heinz, *Phys. Rev. Lett.* **2009**, *102*, 256405.

[71] K. S. Novoselov, A. K. Geim, S. V. Morozov, D. Jiang, Y. Zhang, S. V. Dubonos, I. V. Grigorieva, A. A. Firsov, *Science* **2004**, *306*, 666.

[72] H.-C. Chang, Y.-J. Huang, H.-Y. Chang, W.-J. Su, Y.-T. Shih, Y.-S. Huang, K.-Y Lee, *Appl. Phys. Express* **2014**, *7*, 055101.

[73] S. Das, P. Sudhagar, E. Ito, D. Lee, S. Nagarajan, S.Y. Lee, Y.S. Kang, W. Choi, *J. Mater. Chem.* **2012**, *22*, 20490.

[74] F. Chaabouni, M. Abaab, B. Rezig, *Sensors and Actuators B: Chemical* **2004**, *100*, 200.

[75] L. D'Arsié, S. Esconjauregui, R. S. Weatherup, X. Wu, W. E. Arter, H. Sugime, C. Cepekb, J. Robertson, *RSC Adv.* **2016**, *6*, 113185.

[76] A. C. Crowther, A. Ghassaei, N. Jung, L. E. Brus, *ACS Nano* **2012**, *6*, 1865.

[77] W. Yuan, L. Huang, Q. Zhou, G. Shi, *ACS Appl. Mater. Interfaces* **2014**, *6*, 17003.

[78] T. O. Wehling, K. S. Novoselov, S. V. Morozov, E. E. Vdovin, M. I. Katsnelson, A. K. Geim, A. I. Lichtenstein, *Nano Lett.* **2008**, *8*, 173.

[79] N. Jung, N. Kim, S. Jockusch, N.J. Turro, P. Kim, L. Brus, *Nano Lett.* **2009**, *9*, 4133.

[80] S. Tongay, K. Berke, M. Lemaitre, Z. Nasrollahi, D.B. Tanner, A.F. Hebard, B.R. Appleton, *Nanotechnology* **2011**, *22*, 425701.

[81] W. Chen, S. Chen, D.C. Qi, X.Y. Gao, A.T.S. Wee, *J. Am. Chem. Soc.* **2007**, *129*, 10418.

[82] H. Pinto, R. Jones, J.P. Goss, P.R. Briddon, Journal of Physics: Condensed Matter **2009**, *21*, 402001.

[83] X. Dong, D. Fu, W. Fang, Y. Shi, P. Chen, L. Li, *Small*, **2009**, *5*, 1422.

[84] A. Das, S. Pisana, B. Chakraborty, S. Piscanec, S.K. Saha, U.V. Waghmare, K.S. Novoselov, H.R. Krishnamurthy, A.K. Geim, A.C. Ferrari, A.K. Sood, Nat. Nanotechnol. **2008**, *3*, 210.

[85] Y.H. Lu, W. Chen, Y.P. Feng, P.M. He, J. Phys. Chem. B **2009**, *113*, 2.

[86] O. Sul, K. Kim, E. Choi, J. Kil, W. Park, S. Lee, Nanotechnology **2016**, *27*, 505205.

[87] T. Feng, D. Xie, H. Zhao, G. Li, J. Xu, T. Ren, H. Zhu, Carbon **2014**, *77*, 424.

[88] G. Giovannetti, P.A. Khomyakov, G. Brocks, V.M. Karpan, J. van den Brink, P.J. Kelly, *Phys. Rev. Lett.* **2008**, *101*, 26803.

[89] Z. Chen, I. Santoso, R. Wang, L.F. Xie, H.Y. Mao, H. Huang, Y.Z. Wang, X.Y. Gao, Z.K. Chen, D. Ma, A.T.S. Wee, W. Chen, *Appl. Phys. Lett.* **2010**, *96*, 213104.

[90] F. Güneş, H. Shin, C. Biswas, G.H. Han, E.S. Kim, S.J. Chae, J. Choi, Y.H. Lee, *ACS Nano* **2010**, *4*, 4595.

[91] C. Oshimayx, A. Nagashima, *J. Phys.: Condens. Matter* **1997**, *9*, 1.

[92] J. Dai, J. Yuan, P. Giannozzi, *Appl. Phys. Lett.* **2009**, *95*, 232105.

[93] S. Lee, S.-O. Kim, H. Shin, H.-J. Yun, K. Yang, S.-K. Kwon, J.-J. Kim, Y.-H. Kim, *J. Am. Chem. Soc.* **2013**, *135*, 14321.

[94] L. Xie, X. Wang, H. Mao, Rui Wang, M. Ding, Y. Wang, B. Özyilmaz, K. P. Loh, A. T. S. Wee,

Ariando, W. Chen, *Appl. Phys. Lett.* **2011**, *99*, 012112.

[95] D.-C. Choi, M. Kim, Y. J. Song, S. Hussain, W.-S. Song, K.-S. Ane, J. Jung, *Appl. Surf. Sci.* **201**7, *7*, 301.

[96] L. Duan, Y. Zhang, X. Cheng, Y. Zhang, W. Zhang, J. Wang, F. Han, *Optik-International Journal for Light and Electron Optics* **2018**, *154*, 177.

[97] X. Meng, S. Tongay, J. Kang, Z. Chen, F. Wu, S. Li, J. Xia, J. Li, J. Wu, *Carbon* **2013**, *57*, 507.

[98] N.A. Vinogradov, K.A. Simonov, A.V. Generalov, A.S. Vinogradov, D.V. Vyalikh, C. Laubschat, N. M Rtensson, A.B. Preobrajenski, I.F.R.F. Astronomi, Y.O.G. Nsskiktsvetenskap, T.V. Det, U. Universitet, F. Sektionen, *J. Physics. Condens. Matter* **2012**, *24*, 314202.

[99] W. Zhao, P.H. Tan, J. Liu, A.C. Ferrari, *J. Am. Chem. Soc.* **2011**, *133*, 5941.

[100] I. Khrapach, F. Withers, T. H. Bointon, D. K. Polyushkin, W. L. Barnes, S. Russo, M. F. Craciun, *Adv. Mater.* **2012**, *24*, 2844.

[101] D. J. Wehenkel, T. H. Bointon, T. Booth, P. Bøggild, M. F. Craciun, S. Russo, *Sci. Rep.* **2015**, *5*, 7609.

[102] T. H. Bointon, S. Russo, M. F. Craciun, *IET Circuits Devices Syst.* **2015**, *9*, 403.

[103] C.W. Jang, J.M. Kim, J.H. Kim, D.H. Shin, S. Kim, S. Choi, *J. Alloy. Compd* **2015**, *621*, 1.

[104] Z. Xiea, R. Yao, Y. Zhang, Z. Zhang, Y. Zhang, W. Gao, L. Duan, *Physica B: Condensed Matter* **2019**, *558*, 1.

[105] H. Wang, Y. Zhou, D. Wu, L. Liao, S. Zhao, H. Peng, Z. Liu, *Small* **2013**, *9*, 1316.

[106] X. Li, L. Fan, Z. Li, K. Wang, M. Zhong, J. Wei, D. Wu, H. Zhu, *Adv. Energy Mater* **2012**, *2*, 425.

[107] T. Wu, H. Shen, L. Sun, B. Cheng, B. Liu, J. Shen, *New J. Chem.* **2012**, *36*, 1385.

[108] Pooja Rani, V. K. Jindal, *RSC Adv.* **2013**, *3*, 802.

[109] R.H. Miwa, T.B. Martins, A. Fazzio, *Nanotechnology* **2008**, *19*, 155708.

[110] R. Faccio, L. Fernández-Werner, H. Pardo, C. Goyenola, O.N. Ventura, Á.W. Mombrú, *The Journal of Physical Chemistry C* **2010**, *114*, 18961.

[111] H. Gao, Z. Liu, L. Song, W. Guo, W. Gao, L. Ci, A. Rao, W. Quan, R. Vajtai, P.M. Ajayan, *Nanotechnology* **2012**, *23*, 275605.

[112] C. Liang, Y. Wang and T. Li, *Carbon*, **2015**, *82*, 506.

[113] H. Choi, H. Jo, S. Hwang, M. Jeon, J. Kim, *J. Korean Phys. Soc.* **2016**, *68*, 1257.

[114] M. Chen, H. Zhou, C. Qiu, H. Yang, F. Yu, L. Sun, *Nanotechnology* **2012**, *23*, 115706.

[115] X. Zhang, A. Hsu, H. Wang, Y. Song, J. Kong, M.S. Dresselhaus, T. Palacios, *ACS Nano* **2013**, *7*, 7262.

[116] J. Yan, Y. Zhang, P. Kim, A. Pinczuk, *Phys. Rev. Lett.* **2007**, *98*, 166802.

[117] S. Pisana, M. Lazzeri, C. Casiraghi, K.S. Novoselov, A.K. Geim, A.C. Ferrari, F. Mauri, *Nat. Mater.* **2007**, *6*, 198.

[118] Z.H. Ni, T. Yu, Z.Q. Luo, Y.Y. Wang, L. Liu, C.P. Wong, J. Miao, W. Huang, Z.X. Shen, *ACS Nano* **2009**, *3*, 569.

[119] M. Zhong, D. Xu, X. Yu, K. Huang, X. Liu, Y. Qu, Y. Xu, D. Yang, *Nano Energy* **2016**, *28*, 12.

[120] Z. Wang, W. Wang, M. Wang, X. Meng, J. Li, *J. Mater. Sci.* **2013**, *48*, 2284.

[121] L. Wang, Z. Sofer, P. Šimek, I. Tomandl, M. Pumera, *J. Phys. Chem. C* **2013**, *117*, 23251.

[122] Q. Zhu, J. Yu, W. Zhang, H. Dong, L. Dong, *Journal of Renewable and Sustainable Energy* **2013**, *5*, 021408.

[123] X. Wang, L. Zou, D. Li, Q. Zhang, F. Wang, Z. Zhang, *J. Phys. Chem. C* **2015**, *119*, 1061.

[124] A. Dianat, Z. Liao, M. Gall, T. Zhang, R. Gutierrez, E. Zschech, G. Cuniberti, *Nanotechnology* **2017**, *28*, 215701.

[125] G. F. Jones, R. M. Pinto, A. De Sanctis, V. K. Nagareddy, C. D. Wright, H. Alves, M. F. Craciun, S. Russo, *Adv. Mater.* **2017**, *29*, 1702993.

[126] J. Zabel, R.R. Nair, A. Ott, T. Georgiou, A.K. Geim, K.S. Novoselov, C. Casiraghi, *Nano Lett.* **2012**, *12*, 617.

[127] A. K. Geim, K. S. Novoselov, *Nature* **2007**, *6*, 183.

[128] H. Masujima, T. Mori, Y. Hayamizu, *J. Electron. Mater.* **2017**, *46*, 4463.

[129] X. Wang, X. Li, L. Zhang, Y. Yoon, P.K. Weber, H. Wang, J. Guo, H. Dai, *Science* **2009**, *324*, 768.

[130] S. Kim, P. Zhao, S. Aikawa, E. Einarsson, S. Chiashi, S. Maruyama, *ACS Appl. Mater. Inter*. **2015**, *7*, 9702.

[131] W. Xu, L. Wang, Y. Liu, S. Thomas, H. Seo, K. Kim, K.S. Kim, T. Lee, *Adv. Mater.* **2015**, *27*, 1619.

[132] P. Ho, Y. Yeh, D. Wang, S. Li, H. Chen, Y. Chung, C. Lin, W. Wang, C. Chen, *ACS Nano* **2012**, *6*, 6215.

[133] S. Some, J. Kim, K. Lee, A. Kulkarni, Y. Yoon, S. Lee, T. Kim, H. Lee, *Adv. Mater.* **2012**, *24*, 5481.

[134] H. Park, J. Yoon, J. Jeon, J. Kim, S. Jo, H. Yu, S. Lee, J. Park, *Org. Electron.* **2015**, *22*, 117.

[135] P. Bhunia, E. Hwang, Y. Yoon, E. Lee, S. Seo, H. Lee, *Chemistry-A European Journal* **2012**, *18*, 12207.

[136] C. Li, C. Chueh, F. Ding, H. Yip, P. Liang, X. Li, A.K.Y. Jen, *Adv. Mater.* **2013**, *25*, 4425.

[137] W. Qian, X. Cui, R. Hao, Y. Hou, Z. Zhang, *ACS Appl. Mater. Inter*. **2011**, *3*, 2259.

[138] H. Wang, T. Maiyalagan, X. Wang, *ACS Catal*. **2012**, *2*, 781.

[139] T. Schiros, D. Nordlund, L. Pálová, D. Prezzi, L. Zhao, K.S. Kim, U. Wurstbauer, C. Gutiérrez, D. Delongchamp, C. Jaye, D. Fischer, H. Ogasawara, L.G.M. Pettersson, D.R. Reichman, P. Kim, M.S. Hybertsen, A.N. Pasupathy, *Nano Lett.* **2012**, *12*, 4025.

[140] D. Wei, Y. Liu, Y. Wang, H. Zhang, L. Huang, G. Yu, *Nano Lett.* **2009**, *9*, 1752.

[141] B. Guo, Q. Liu, E. Chen, H. Zhu, L. Fang, J.R. Gong, *Nano Lett.* **2010**, *10*, 4975.

[142] Y. Lu, S. Lo, J. Lin, W. Zhang, J. Lu, F. Liu, C. Tseng, Y. Lee, C. Liang, L. Li, *ACS Nano* **2013**, *7*, 6522.

[143] D.W. Chang, E.K. Lee, E.Y. Park, H. Yu, H. Choi, I. Jeon, G. Sohn, D. Shin, N. Park, J.H. Oh, L. Dai, J. Baek, *J. Am. Chem. Soc.* **2013**, *135*, 8981.

[144] Z. Wang, P. Li, Y. Chen, J. Liu, H. Tian, J. Zhou, W. Zhang, Y. Li, *J. Mater. Chem. C* **2014**, *2*, 7396.

[145] C. Zhang, W. Lin, Z. Zhao, P. Zhuang, L. Zhan, Y. Zhou, W. Cai, *Science China Physics, Mechanics & Astronomy* **2015**, *58*.

[146] A. Wei, J. Wang, Q. Long, X. Liu, X. Li, X. Dong, W. Huang, *Mater. Res. Bull.* **2011**, *46*, 2131.

[147] X. Li, T. Tang, M. Li, X. He, *Appl. Phys. Lett.* **2015**, *106*, 13110.

[148] Y. Lin, C. Lin and P. Chiu, *Appl. Phys. Lett.*, **2010**, *96*, 133110.

[149] Y. Xue, B. Wu, H. Liu, J. Tan, W. Hu, Y. Liu, *Phys. Chem. Chem. Phys.* **2014**, *16*, 20392.

[150] I. Nikiforidis, I. Karafyllidis, P. Dimitrakis, *J. Phys. D: Appl. Phys.* **2018**, *51*, 075303.

[151] S. Grover, A. Joshi, A. Tulapurkar, M.M. Deshmukh, *Sci Rep.* **2017**, *7*, 3336.

[152] M.C. Lemme, F.H.L. Koppens, A.L. Falk, M.S. Rudner, H. Park, L.S. Levitov, C.M. Marcus, *Nano Lett.* **2011**, *11*, 4134.

[153] J. Ye, M. F. Craciun, M. Koshino, S. Russo, S. Inoue, H. Yuan, H. Shimotani, A. F. Morpurgo, Y. Iwasa, *Proceedings of the national academy of sciences of the United States of America* **2011**, *108*, 13002.

[154] J.R. Williams, L. DiCarlo, C.M. Marcus, *Science* **2007**, *317*, 638.

[155] S. Chen, Z. Han, M.M. Elahi, K.M.M. Habib, L. Wang, B. Wen, Y. Gao, T. Taniguchi, K. Watanabe, J. Hone, A.W. Ghosh, C.R. Dean, *Science* **2016**, *353*, 1522.

[156] A. Hammam, M. Schmidt, M. Muruganathana, H. Mizuta, *Carbon* **2017**, *121*, 399.

[157] G. Liu, J. Velasco, W. Bao, C.N. Lau, *Appl. Phys. Lett.* **2008**, *92*, 203103.

[158] G. Rao, M. Freitag, H. Chiu, R.S. Sundaram, P. Avouris, *ACS Nano* **2011**, *5*, 5848.

[159] E.C. Peters, E.J.H. Lee, M. Burghard, K. Kern, *Appl. Phys. Lett.* **2010**, *97*, 193102.

[160] J. Liu, S. Safavi-Naeini, D. Ban, *Electronics Lett.* **2014**, *50*, 1724.

[161] N.S. Moghaddam, M.T. Ahmadi, M. Rahmani, N.A. Amin, H.S. Moghaddam, R. Ismail, *Journal of Nanoengineering and Nanomanufacturing* **2012**, *2*, 375.

[162] B.H. Seo, J. Youn, M. Shim, *ACS Nano*, **2014**, *8*, 8831.

[163] X. Yu, Y. Shen, T. Liu, T. Wu, Q. Jie Wang, *Sci. Rep.* **2015**, *5*.

[164] M. Freitag, T. Low, P. Avouris, *Nano Lett.* **2013**, *13*, 1644.

[165] K. Yan, D. Wu, H. Peng, L. Jin, Q. Fu, X. Bao, Z. Liu, *Nat. Commun*. **2012**, *3*.

[166] S. Wang, Y. Sekine, S. Suzuki, F. Maeda, H. Hibino, *Nanotechnology* **2015**, *26*, 385203.

[167] J. Baltazar, H. Sojoudi, S.A. Paniagua, J. Kowalik, S.R. Marder, L.M. Tolbert, S. Graham, C.L. Henderson, *J. Phys. Chem. C* **2012**, *116*, 19095.

[168] A. De Sanctis, G. F. Jones, D. J. Wehenkel, F. Bezares, F. H. L. Koppens, M. F. Craciun, S. Russo, *Sci. Adv.* **2017**, *3*, e1602617.

[169] Tony Low, *Phys. Rev. B* **2009**, *80*, 205423.

[170] H. Tian, J. Wang, *J. Phys.: Condens. Matter* **2017**, *29*, 385401.

[171] S. Cheng, *J. Phys. : Condens. Matter* **2018**, *30*, 165301.

[172] M.Z. Iqbal, S. Siddique, M.W. Iqbal, J. Eom, *J. Mater Chem C.* **2013**, *1*, 3078.

[173] M.W. Jung, W.S. Song, S. Myung, J.S. Lim, S.S. Lee, K.S. An, *Advanced Materials Research* **2015**, *1098*, 63.

[174] L.K. Putri, B. Ng, W. Ong, H.W. Lee, W.S. Chang, S. Chai, *J. Mater. Chem. A* **2018**, *6*, 3181.

[175] M. Latorre-Sánchez, A. Primo, P. Atienzar, A. Forneli, H. García, *Small* **2015**, *11*, 970.

[176] C.O. Kim, S. Kim, D.H. Shin, S.S. Kang, J.M. Kim, C.W. Jang, S.S. Joo, J.S. Lee, J.H. Kim, S. Choi, E. Hwang, *Nat. Commun.* **2014**, *5*.

[177] S. Kim, D.H. Shin, C.O. Kim, S.S. Kang, J.M. Kim, C.W. Jang, S.S. Joo, J.S. Lee, J.H. Kim, S. Choi, E. Hwang, *ACS Nano* **2013**, *7*, 5168.

Pin Tian is an assistant engineer in Kunming Institute of Physics. He received his Bachelor of Science and Master of Science from Yunnan Normal University and Yunnan University in 2014 and 2017, respectively. His current research focuses on fabrication of two-dimensional materials and infrared photodetectors.

Prof. Libin Tang *received his Bachelor and Master degrees in Applied Chemistry and Physical Chemistry from Yunnan University in 2000 and 2003, respectively. He received his PhD in optical engineering from Kunming Institute of Physics at China in 2009 and worked as postdoctoral fellow in the Department of Applied Physics at Hong Kong Polytechnic University between 2010 and 2014. He was promoted to Professor at Kunming Institute of Physics in 2013. Currently, he is the Innovation Team Leader and Director of Kunming Key*

Laboratory of Graphene Photoelectric Materials & Devices. His research interest is in graphene, 2D materials and optoelectronics.

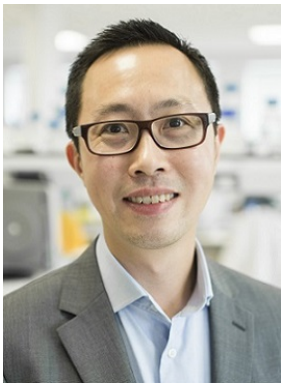

Prof. Kar Seng Teng received his Bachelor of Engineering and PhD in Electrical and Electronic Engineering from Swansea University at the United Kingdom in 1997 and 2001, respectively. Currently, he leads the Nanoelectronics Research Group at the College of Engineering at Swansea University. His research interest is in the study of nanoscale electronic materials and devices. This involves the application of nanotechnology in electronics, which has major impact on healthcare, photonics and energy technologies.

Jin-Zhong Xiang, Professor, Yunnan University, born in 1963, in Sui County, Henan Province, P. R. China. He received a Bachelor of Science, specializing in Magnetism, from the Physics Department of Lanzhou University in 1983. Subsequently, he received a Master of Science in Nuclear Physics and Ph.D. in Condensed Matter Physics in 1986 and 1991, respectively. At present, he mainly engages in the research of photoelectric materials and device physics, and in low-dimensional materials and nanotechnology etc.

Shu Ping Lau is a full professor and Head of Department of Applied Physics at the Hong Kong Polytechnic University. He is also the Director of the University Research Facility on Materials Characterization and Device Fabrication. He obtained his Ph.D degree in Materials Engineering from the University of Swansea. His current research interest includes two-dimensional materials and graphene quantum dots.

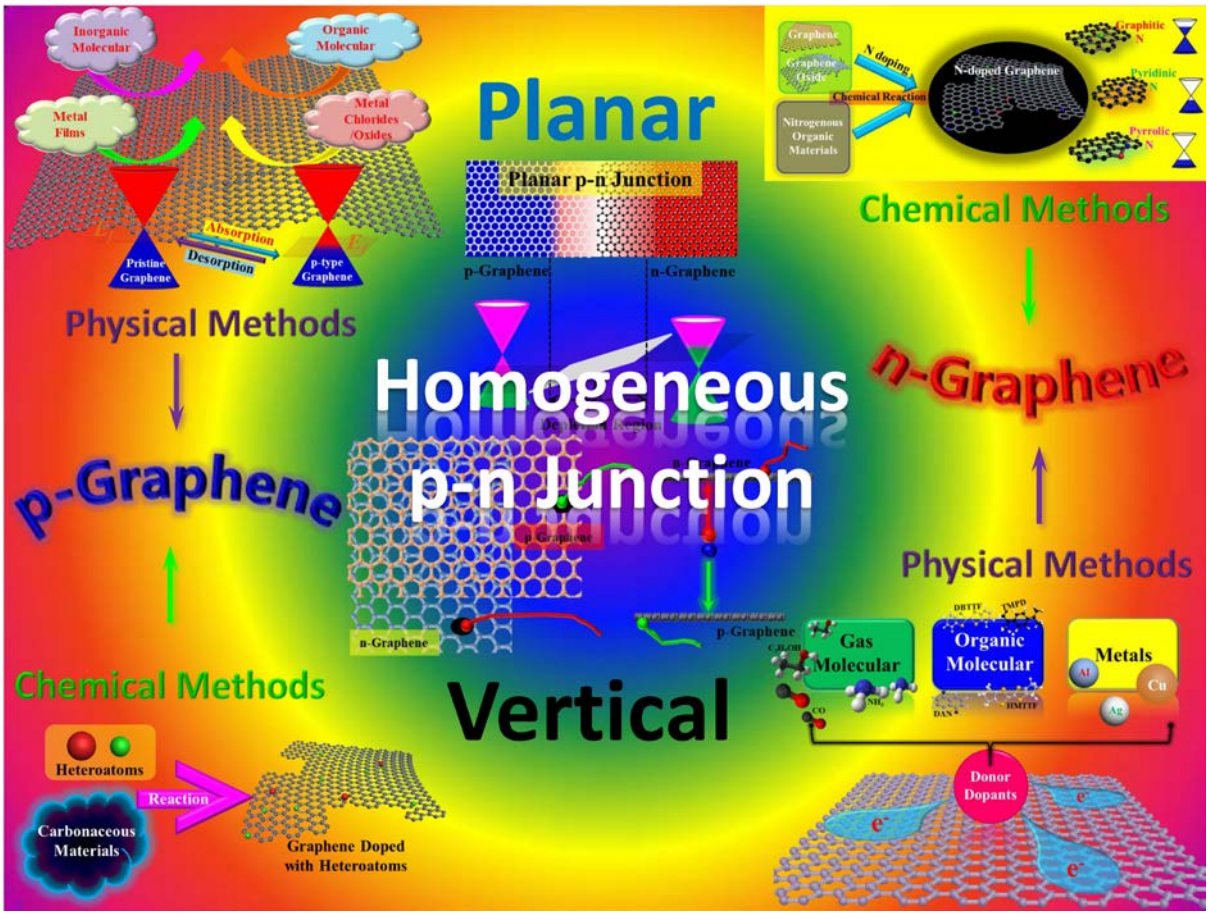
Inorganic Molecular
Organic Molecular
Metal Films
Metal Chlorides /Oxides
Absorption
Desorption
Pristine Graphene
p-type Graphene
Physical Methods
p-Graphene
Chemical Methods
Heteroatoms
Reaction
Carbonaceous Materials
Graphene Doped with Heteroatoms
Planar
Planar p-n Junction
p-Graphene
n-Graphene
Homogeneous p-n Junction
Vertical
Graphene
Graphene Oxide
N doping
Chemical Reaction
Nitrogenous Organic Materials
N-doped Graphene
Graphitic N
Pyridinic N
Pyrrolic N
Chemical Methods
n-Graphene
Physical Methods
Gas Molecular
Organic Molecular
Metals
Donor Dopants